

Radiative forcing in the 21st century due to ozone changes in the troposphere and the lower stratosphere

M. Gauss,¹ G. Myhre,¹ G. Pitari,² M. J. Prather,³ I. S. A. Isaksen,¹ T. K. Berntsen,¹ G. P. Brasseur,⁴ F. J. Dentener,⁵ R. G. Derwent,⁶ D. A. Hauglustaine,⁷ L. W. Horowitz,⁸ D. J. Jacob,⁹ M. Johnson,¹⁰ K. S. Law,¹⁰ L. J. Mickley,⁹ J.-F. Müller,¹¹ P.-H. Plantévin,¹⁰ J. A. Pyle,¹⁰ H. L. Rogers,¹⁰ D. S. Stevenson,¹² J. K. Sundet,¹ M. van Weele,¹³ and O. Wild¹⁴

Received 6 June 2002; revised 6 November 2002; accepted 7 March 2003; published 13 May 2003.

[1] Radiative forcing due to changes in ozone is expected for the 21st century. An assessment on changes in the tropospheric oxidative state through a model intercomparison (“OxComp”) was conducted for the IPCC Third Assessment Report (IPCC-TAR). OxComp estimated tropospheric changes in ozone and other oxidants during the 21st century based on the “SRES” A2p emission scenario. In this study we analyze the results of 11 chemical transport models (CTMs) that participated in OxComp and use them as input for detailed radiative forcing calculations. We also address future ozone recovery in the lower stratosphere and its impact on radiative forcing by applying two models that calculate both tropospheric and stratospheric changes. The results of OxComp suggest an increase in global-mean tropospheric ozone between 11.4 and 20.5 DU for the 21st century, representing the model uncertainty range for the A2p scenario. As the A2p scenario constitutes the worst case proposed in IPCC-TAR we consider these results as an upper estimate. The radiative transfer model yields a positive radiative forcing ranging from 0.40 to 0.78 W m⁻² on a global and annual average. The lower stratosphere contributes an additional 7.5–9.3 DU to the calculated increase in the ozone column, increasing radiative forcing by 0.15–0.17 W m⁻². The modeled radiative forcing depends on the height distribution and geographical pattern of predicted ozone changes and shows a distinct seasonal variation. Despite the large variations between the 11 participating models, the calculated range for normalized radiative forcing is within 25%, indicating the ability to scale radiative forcing to global-mean ozone column change. *INDEX TERMS:* 0365 Atmospheric Composition and Structure: Troposphere—composition and chemistry; 0341 Atmospheric Composition and Structure: Middle atmosphere—constituent transport and chemistry (3334)

Citation: Gauss, M., et al., Radiative forcing in the 21st century due to ozone changes in the troposphere and the lower stratosphere, *J. Geophys. Res.*, 108(D9), 4292, doi:10.1029/2002JD002624, 2003.

¹Department of Geophysics, University of Oslo, Norway.

²Dipartimento di Fisica, Università de L'Aquila, Coppito, L'Aquila, Italy.

³Earth System Science Department, University of California at Irvine, Irvine, California, USA.

⁴Max-Planck-Institut für Meteorologie, Hamburg, Germany.

⁵Joint Research Centre, Climate Change Unit, Ispra, Italy.

⁶UK Met Office, Climate Research Division, Berks, UK.

⁷Institut Pierre Simon Laplace, Gif-sur-Yvette, France.

⁸Geophysical Fluid Dynamics Laboratory, NOAA, Princeton University, Princeton, New Jersey, USA.

⁹Department of Earth and Planetary Sciences, Harvard University, Cambridge, Massachusetts, USA.

¹⁰Chemistry Department, Cambridge University, Cambridge, UK.

¹¹IASB, Brussels, Belgium.

¹²Institute for Meteorology, University of Edinburgh, Edinburgh, UK.

¹³Royal Netherlands Meteorological Institute (KNMI), De Bilt, Netherlands.

¹⁴Frontier Research System for Global Change, Yokohama, Japan.

1. Introduction

[2] Ozone plays a central role in the radiative budget of the atmosphere through its interaction with both shortwave and longwave radiation. Being the precursor for key oxidizing agents in the troposphere, essentially OH and NO₃, ozone strongly influences the lifetime of other greenhouse gases such as methane and HCFCs, thus providing an additional, indirect impact on climate. Taking into account only the direct effect of ozone change, the “Intergovernmental Panel on Climate Change (IPCC)” estimates tropospheric ozone to provide the third largest positive radiative forcing since the preindustrial era [Ramaswamy *et al.*, 2001].

[3] Given the thermal structure of the atmosphere and horizontally varying quantities such as cloudiness and surface albedo, radiative forcing induced by changes in ozone will strongly depend on the location where the ozone change occurs. Owing to the absorption of shortwave radiation from the Sun (UV) and the absorption and

emission of longwave radiation from the earth, increases in lower stratospheric ozone imply a negative shortwave and a positive longwave radiative forcing, while tropospheric ozone increases lead to a positive radiative forcing in both the shortwave and longwave spectral regions. The strong dependence of radiative forcing on the altitude of the ozone change is pointed out in several studies [Wang and Sze, 1980; Lacis et al., 1990; Forster and Shine, 1997; Hansen et al., 1997]. Berntsen et al. [1997] explore the horizontal variation of radiative forcing due to ozone change since preindustrial times and find distinctive horizontal patterns for both the shortwave and longwave components.

[4] As opposed to the long-lived and well-mixed greenhouse gases (CO_2 , CH_4 , halocarbons, and N_2O), ozone has a short chemical lifetime compared to transport timescales in the troposphere and thus exhibits a highly spatially inhomogeneous distribution. Therefore its global radiative forcing cannot be derived from local observations and the knowledge of its radiative properties. Given the difficulty of measuring tropospheric ozone continuously and with global coverage, atmospheric chemistry models have been developed and used extensively during the last few decades in order to simulate its three-dimensional (3-D) distributions as a function of time.

[5] Increases in tropospheric ozone since the preindustrial period are calculated to have led to significant radiative forcing. Kiehl et al. [1999] find a radiative forcing of 0.30 W m^{-2} for the period 1870–1990 due to increases in tropospheric ozone, whereas Berntsen et al. [2000] calculate 0.34 W m^{-2} for the period 1850–1990 and Hauglustaine and Brasseur [2001] derive a value of 0.43 W m^{-2} for the period 1850–2000. Mickley et al. [2001] point to the uncertainty in preindustrial ozone levels and obtain an instantaneous radiative forcing as much as $0.72\text{--}0.80 \text{ W m}^{-2}$, which would make ozone at least as important as methane. Chapter 6 of the “IPCC Third Assessment Report (IPCC-TAR)” [Ramaswamy et al., 2001] focuses on the period 1750–1998 and reports a radiative forcing of $0.35 \pm 0.15 \text{ W m}^{-2}$ caused by the increase in tropospheric ozone, compared to 2.43 W m^{-2} due to the well-mixed greenhouse gases (CO_2 , 1.46 W m^{-2} ; CH_4 , 0.48 W m^{-2} ; CFCs, 0.34 W m^{-2} ; and N_2O , 0.15 W m^{-2}). As an estimate for the radiative forcing due to the ozone loss in the lower stratosphere during the 1979–1997 period, the IPCC-TAR adopts a net radiative forcing of $-0.15 \pm 0.1 \text{ W m}^{-2}$ (the negative longwave effect being more significant than the positive shortwave effect), compared to $-0.10 \pm 0.02 \text{ W m}^{-2}$ found by Forster [1999], -0.10 W m^{-2} found by Myhre et al. [2001], and -0.01 W m^{-2} calculated for the period since 1970 by Kiehl et al. [1999].

[6] As pointed out by various publications [e.g., WMO, 1999] human impact will lead to a further enhancement of ozone in the troposphere in the decades to come, at the same time as stratospheric ozone is expected to recover largely as a response to decreasing chlorine and bromine levels. Clearly, the radiative forcing due to future ozone change in the stratosphere and its significance compared to the forcing by tropospheric ozone changes will depend on the rate of recovery of the ozone layer and the spatial structure of such a recovery in midlatitudes and high latitudes. Several works have been published on radiative forcing due to future tropospheric ozone changes. For example, Chalita et al. [1996] obtain a globally averaged radiative forcing of 0.15 W m^{-2} for the period 1990–2050, while the models

of van Dorland et al. [1997] and Brasseur et al. [1998a] suggest higher values of 0.28 and 0.27 W m^{-2} , respectively. Stevenson et al. [1998a] calculate a radiative forcing of 0.48 W m^{-2} for 1990–2100, using a $2 \times \text{CO}_2$ climate. All these studies apply the IS92a scenario for future surface emissions. For the “IPCC Special Report on Emission Scenarios (SRES)” [Nakicenovic et al., 2000] A2p and B2p scenarios Stevenson et al. [2000] find radiative forcings of 0.43 and 0.22 W m^{-2} , respectively, for 1990–2100 assuming a fixed climate. Differences in these calculations are likely to be due to modeled differences in the spatial distributions or the magnitudes of projected O_3 changes, which in turn are a result of different emission inventories or processes such as chemistry and transport used in the models.

[7] This paper focuses on ozone changes and the resulting radiative forcing to be expected for the 21st century. For chapter 4 of the IPCC-TAR [Prather et al., 2001], research groups involved in 3-D global tropospheric chemistry modeling were invited to participate in an assessment of the change in the tropospheric oxidative state through a model intercomparison (“OxComp”). Stationary experiments were performed for the years 2000 and 2100, yielding estimates for tropospheric ozone change to be expected for the 21st century. In the present study, these estimates are taken as input for detailed radiative transfer calculations in order to assess the ozone-induced radiative forcing for the period 2000–2100. Given the uncertainties of model predictions going that far into the future, combined with the strong dependence of radiative forcing on the spatial distribution and magnitude of ozone change, we evaluate results from a variety of 11 chemical transport models (CTMs) in order to improve the confidence level beyond what could be obtained from a single model study. The chosen models use different transport schemes, chemistry packages, and meteorological input data. Also, the horizontal and vertical resolutions are highly variable among the models. In OxComp, a high emission scenario was used for the year 2100 in order to obtain an upper limit for the estimated change in ozone and other chemical key components. However, since the focus of OxComp was on tropospheric ozone changes while keeping stratospheric chemistry largely unchanged, the question remained whether or not stratospheric ozone changes will make a significant contribution to radiative forcing in the future. To answer this question, two participating groups present two additional experiments in this paper, where the stratosphere is allowed to respond freely to changes in ozone precursors and ozone depleting agents. It has to be emphasized, however, that all model experiments used in this study use the same meteorology for 2000 and 2100, i.e., no climate feedback mechanism is taken into account.

[8] The calculated 3-D changes in ozone between the surface and 20 km are used as input in the radiative transfer model. The longwave and shortwave radiative forcings are considered separately. The spatial distribution and seasonal variation of radiative forcing and normalized radiative forcing are calculated for the 11 data sets of ozone change. The role of model uncertainties in the prediction of ozone changes for radiative forcing calculations is investigated in detail.

[9] The following section will briefly describe the CTMs and discuss the results from OxComp as well as from the two additional experiments focusing on the importance of

Table 1. Emissions Specified for OxComp for the Year 2000 and 2100 Simulations^a

Species	2000	2100
CH ₄	prescribed to 1745 ppbv in the troposphere	prescribed to 4300 ppbv in the troposphere ^b
NO _x	fossil fuel combustion: 31.7 Tg(N) yr ⁻¹ biomass burning: 7.1 Tg(N) yr ⁻¹ aircraft: 0.7 Tg(N) yr ⁻¹ (1992 emissions augmented by a factor 1.37) lightning: 5 Tg(N) yr ⁻¹ soil, natural: 5.6 Tg(N) yr ⁻¹ total: 50.1 Tg(N) yr ⁻¹	fossil fuel combustion: 108.8 Tg(N) yr ⁻¹ biomass burning: 7.1 Tg(N) yr ⁻¹ aircraft: 2.17 Tg(N) yr ⁻¹ (1992 emissions augmented by a factor 4.34) lightning: same as 2000 ^c soil, natural: same as 2000 ^c total: 128.7 Tg(N) yr ⁻¹
CO	oxidation (methane, isoprene, etc): model dependent vegetation: 150 Tg(CO) yr ⁻¹ oceans: 50 Tg(CO) yr ⁻¹ biomass burning: 700 Tg(CO) yr ⁻¹ fossil fuel combustion: 650 Tg(CO) yr ⁻¹ total: 1550 Tg(CO) yr ⁻¹ (excluding oxidation)	oxidation (methane, isoprene, etc): model dependent vegetation: same as 2000 ^c oceans: same as 2000 ^c biomass burning: same as 2000 ^c fossil fuel combustion: 2098 Tg(CO) yr ⁻¹ total: 2998 Tg(CO) yr ⁻¹ (excluding oxidation)
NMHC	isoprene: 220 Tg(C) yr ⁻¹ terpene: 127 Tg(C) yr ⁻¹ acetone: 30 Tg(C) yr ⁻¹ fossil fuel combustion: 161 Tg(C) yr ⁻¹ biomass burning: 33 Tg(C) yr ⁻¹ total: 571 Tg(C) yr ⁻¹	isoprene: same as 2000 ^c terpene: same as 2000 ^c acetone: same as 2000 ^c fossil fuel combustion: 322 Tg(C) yr ⁻¹ biomass burning: same as 2000 ^c total: 732 Tg(C) yr ⁻¹
NH ₃	oceans: 8.2 Tg(N) yr ⁻¹ soil/vegetation: 2.4 Tg(N) yr ⁻¹ anthropogenic: 46.7 Tg(N) yr ⁻¹ (1990 emissions augmented by a factor 1.095) total: 57.3 Tg(N) yr ⁻¹	oceans: same as 2000 ^c soil/vegetation: same as 2000 ^c anthropogenic: 111.2 Tg(N) yr ⁻¹ (1990 emissions augmented by a factor 2.6) total: 121.8 Tg(N) yr ⁻¹
N ₂ O ^d	320 ppbv in the troposphere	455 ppbv in the troposphere
CFCs/HCFCs halons ^d	according to WMO [1999]	according to WMO [1999]

^aThe HGIS model used slightly different emissions [see Wang *et al.*, 1998] for year 2000 conditions in order to obtain better agreement with observations. The most important deviations concern biomass burning (12 Tg(N) yr⁻¹, 510 Tg(CO) yr⁻¹), fossil fuel burning (20 Tg(N) yr⁻¹, 390 Tg(CO) yr⁻¹), and isoprene emissions (550 Tg(C) yr⁻¹). All models applied the same “change” of emissions for the 21st century.

^bThe assumed methane levels for 2100 were calculated in a straight integration of the UCI 2D model (M. Prather, personal communication), where the highest SRES scenario was assumed and a chemical feedback factor for methane was included, taking into account the increase of methane lifetime resulting from changes in other chemical components.

^cAlthough natural emissions are likely to change in the future, OxComp decided to use the same natural emissions for 2000 and 2100 since current knowledge is not sufficient for estimating future changes accurately.

^dConcerns only those experiments focusing on both tropospheric and stratospheric changes (section 2.2).

ozone changes in the lower stratosphere. Section 3 will present the results of the radiative transfer calculations in some detail, followed by concluding remarks and suggestions for future directions in section 4.

2. Projection of Ozone Changes in the 21st Century

[10] During the last decade, the use of 3-D models has become common in atmospheric chemistry modeling. The modeling of tropospheric chemistry now takes into account a large number of chemical processes including nonmethane hydrocarbon chemistry. In this analysis we use results from 11 CTMs that participated in OxComp in order to quantify future ozone changes in the troposphere. Two of the models are used to study changes in lower stratospheric ozone in addition.

[11] A detailed description of the experimental setup of OxComp is given in IPCC-TAR [Prather *et al.*, 2001], whereas the following section provides only a brief description of the CTMs and the assumptions that were made with respect to the changes in ozone precursor emissions. The obtained changes in ozone will be discussed in some detail thereafter.

2.1. Tropospheric Ozone Change According to OxComp

[12] Changes in tropospheric ozone are mainly driven by increased emissions of CH₄, carbon monoxide (CO), non-

methane hydrocarbons (NMHCs), and NO_x. In order to estimate changes in tropospheric OH and ozone abundances to occur in the 21st century OxComp performed time slice simulations for the years 2000 and 2100. Anthropogenic emissions used for the year 2000 were taken from the SRES scenarios [Nakicenovic *et al.*, 2000]. Some adjustments had to be made for consistency with current budgets and for the inclusion of natural sources as well as temporal and spatial distributions of emissions that are not specified by SRES. Emissions of NO_x, CO, and VOC were based on extrapolation of the “GEIA (Global Emissions Inventory Activity)/EDGAR” database for 1990 [Graedel *et al.*, 1993; Olivier *et al.*, 1998, 1999], projected to the year 2000, while tropospheric abundances of long-lived gases such as CH₄ were taken from recent observations as listed in Table 4.1 of the IPCC-TAR [Prather *et al.*, 2001]. The emission set for 2100 consisted of the 2000 industrial emissions augmented by the delta emission (2100–2000) provided by the A2p scenario (SRES), which was chosen because it represents the largest increase in emissions of CH₄, CO, NO_x, and VOC, allowing the estimation of an upper limit for the impact on the troposphere. In the simulations for the year 2100, natural emissions were not changed with respect to the year 2000. Table 1 summarizes the main assumptions on emissions in the OxComp experiments.

[13] Shifting the location of emissions has little impact on the distribution of long-lived greenhouse gases, while ozone increases in the troposphere will depend strongly on changes in the geographic pattern of emissions. These changes were

taken from SRES emission maps (scenario A2p). Significantly enhanced industrial emissions of ozone precursors over the Far East constitute the most outstanding feature. By the year 2100, peaks in emissions of NO_x and CO over eastern China are assumed to exceed those over western Europe and northeast US, which increase only slightly over the same period. Enhanced emissions of NO_x , CO, and NMHC are also to be expected over industrialized areas of the South American and African continents. Emissions of NMHC strongly increase in the regions around the Persian Gulf.

[14] The year 2000 simulations were thoroughly tested against sonde measurements of ozone and CO, and detailed results of these comparisons are given in chapter 4 of the IPCC-TAR [Prather *et al.*, 2001]. With the exception of a few outliers the model simulations were within 30% of observed tropospheric ozone abundance, with comparatively large deviations in the upper troposphere. Surface abundances of CO at Cape Grim (40°S) were overestimated by all the models (30–50%), probably indicating an error in Southern Hemisphere emissions of CO. At the other stations, most models are within 30% of the measured CO values. Due to the lack of a more detailed NO_x emission database the models have difficulties in resolving small-scale variations in ozone and CO caused by NO_x . In particular, biomass burning plumes and local thunderstorms are generally poorly represented in global models. By and large, however, the comparison showed good simulations by the OxComp models of the global scale chemical features of the current troposphere as evidenced by these two species.

[15] The main features of the 11 CTMs from which output is used in this study are tabulated in Table 2. The horizontal resolution is highly variable between the models, ranging from $2.8^\circ \times 2.8^\circ$ to 10° latitude \times 22.5° longitude. A large variety of numerical schemes are used for chemistry, advective transport, and convection. The model meteorology is either taken from the “European Centre for Medium-range Weather Forecasts (ECMWF)” or from General Circulation Models (GCMs), which calculate meteorological data from first principles, solar fluxes, and calculated heating and cooling rates.

[16] For the vertical distribution of ozone precursors, in particular, the short-lived NO_x species, convective transport and washout play a crucial role. The parameterizations of these processes differ significantly between the models and are described briefly here. ULAQ applies a scheme for tropospheric deep convection based on Müller and Brasseur [1995] and relates convective uplift rates linearly to the NO_x lightning production calculated by the ECHAM3 GCM [Grewe *et al.*, 2001a]. Washout is calculated from a first-order loss rate using monthly mean precipitation rates from climatological data. UIO1 calculates convection as described by Prather *et al.* [1987]. Large-scale washout is based on zonally and seasonally averaged scavenging rates developed for the Oslo 2-D model [see, e.g., Isaksen and Hov, 1987]. Data from the parent GCM (GISS) are used to calculate longitudinal and temporal dependences.

[17] UCI takes convective mass fluxes for the parent GCM meteorology (GISS 2') and calculates wet deposition from solubilities and large-scale precipitation fields, with additional removal during convection. Deep convection in

IASB follows the scheme of Costen *et al.* [1988]. Washout follows Müller and Brasseur [1995] using climatological precipitation rates and the cloud distribution from the “International Satellite Cloud Climatology Project (ISCCP).” UCAM, UIO2, and KNMI use the mass flux scheme of Tiedtke [1989]. UCAM takes convective and dynamical precipitation from ECMWF reanalysis data, while UIO2 calculates washout based on precipitation rates in the ECMWF forecast data. KNMI couples convective scavenging directly to the ECMWF reanalysis convection following Guelle *et al.* [1998]. In UKMO a fraction of the air parcels between convective cloud top and the ground are completely mixed. The fraction is related to the convective precipitation rate using a factor tuned using Radon-222 profiles [Stevenson *et al.*, 1998b]. Species-dependent scavenging rates are taken from Penner *et al.* [1994]. MOZ1 and MOZ2 use the shallow convection scheme of Hack [1994]. In addition, MOZ2 uses the Zhang and McFarlane [1995] scheme for deep convection. HGIS calculates convective mass flux based on Del Genio and Yao [1993] and employs a prognostic cloud water parameterization that follows the life cycle of water in the atmosphere [Del Genio *et al.*, 1996]. Both MOZ1 and MOZ2 use a first-order loss process within clouds, following Giorgi and Chameides [1985], while HGIS follows the scheme developed by Koch *et al.* [1999] for scavenging of soluble gases.

[18] For OxComp the models used the same meteorology for year 2000 and year 2100 conditions, i.e., no climate feedback was taken into account. The years from which meteorological data was used are given in Table 2. The spin-up length was chosen between 3 and 12 months, followed by 12 months from which results were reported. During the integrations most models used the same meteorology repeatedly for consecutive years. Exceptions are MOZ1 and MOZ2, which used meteorology from successive years of a GCM integration (NCAR CCM-3 and NCAR MACCM-3, respectively), and UCAM, which used ECMWF reanalysis data for 1997 (spin-up) and 1998 (reported).

[19] Since most models are designed for tropospheric studies the focus of OxComp was on tropospheric ozone change, and the issue of stratospheric ozone recovery was left out deliberately (“fixed stratosphere” approach). Most models prescribed the (downward) influx or the mixing ratio of ozone at the model top or at some defined level in the lower stratosphere using the same values for 2000 and 2100. In some models, stratospheric ozone was calculated by a chemical solver, but ozone precursors were kept fixed between 2000 and 2100. All models reported ozone changes from the surface up to 20 km, except UKMO and HGIS, which submitted results up to 14 and 12 km, respectively.

[20] Figures 1a and 1b show annual averages for zonal-mean ozone and NO_x ($\text{NO} + \text{NO}_2$), respectively, calculated for the year 2000. With regard to ozone the agreement among the models is rather good. The mixing ratio amounts to a few tens of ppbv (parts per billion by volume) at the surface and increases with altitude. In low latitudes the ozone contour lines are displaced upward reflecting efficient vertical transport of surface, relatively low ozone air through convection and advection. Differences in ozone may be explained not only by differences in the chemistry modules, but also in the transport of pollutants into remote

Table 2. Chemical Transport Models (CTMs) Contributing to the OxComp Prediction of Tropospheric Ozone Change

CTM	Institute	Contributing Authors	Domain/Resolution	Meteorology	Advection Scheme	Convection Scheme	Chemical Components	Stratospheric Ozone	Spin-Up Length	References
ULLAQ	University of L'Aquila	Pitari	10°lat × 22.5°lon 26 levels, sfc–0.04 hPa	GCM [Pitari, 1993]	Eulerian explicit	described by Pitari <i>et al.</i> [2002], following Müller and Brasseur [1995] described by Prather <i>et al.</i> [1987]	full chemistry, incl. NMHC, PAN, strat/trop aerosols and ozone detailed ozone/NO _x /hydrocarbon scheme including 51 species, QSSA solver	calculated by detailed stratospheric chemistry scheme prescribed 3–5 km above tropopause (influx from stratosphere = 350 Tg yr ⁻¹)	12 months ^a	Pitari <i>et al.</i> [2002]
UJO1	University of Oslo	Berntsen	8°lat × 10°lon nine levels, sfc–10 hPa	GCM (GISS)	second-order moments [Prather, 1986]		ASAD package with NMHC scheme and implicit integrator	influx prescribed at 10 hPa (475 Tg yr ⁻¹)	12 months	Berntsen and Isaksen [1997], Fjøllesvedt <i>et al.</i> [1999]
UCI	University of California, Irvine	Wild	8°lat × 10°lon nine levels, sfc–10 hPa	GCM (GISS 2')	second-order moments [Prather, 1986]	mass fluxes are taken directly from the GISS 2' meteorology	60 species incl. NMHCs	mixing ratio fixed above 50 hPa based on observations	6 months	Wild and Prather [2000], Wild and Akimoto [2001]
IASB	IAS/Belgium	Müller	5° × 5° 25 levels, sfc–50 hPa	monthly means from ECMWF reanalyses (1985–1989 average)	semi-Lagrange [Smolar-kiewicz and Rasch, 1991]	described by Costen <i>et al.</i> [1988]; cumulo-nimbus distribution taken from ISCCP	full chemistry incl. NMHC's and S chemistry	nudged climatological O ₃ profiles, scaled to TOMS columns	12 months	Müller and Brasseur [1995, 1999]
KNMI	KNMI/IMAU Utrecht	van Weele/Dentener	4°lat × 5°lon 19 levels, sfc–10 hPa	ECMWF reanalyses 1993 (ERA15)	slopes scheme [Russel and Lerner, 1981]	mass flux scheme of Tiedtke [1989]		nudged climatological O ₃ profiles, scaled to TOMS columns	12 months	Jeuken <i>et al.</i> [1999], Houweling <i>et al.</i> [2000]
UCAM	Cambridge University	Plantevin/Johnson	5.6° × 5.6° 31 levels, sfc–10 hPa	ECMWF reanalyses 1997/1998	second-order moments [Prather, 1986]	mass flux scheme of Tiedtke [1989]; implementation described by Stockwell and Chipperfield [1999]	O _x , NO _x , HO _x , CH ₄ , simple NMHC scheme, 46 species	specified above 10 hPa	7 months	Law <i>et al.</i> [1998, 2000] (TOMCAT)
MOZI	NCAR/CNRS	Hauglustaine/Brasseur	2.8° × 2.8° 25 levels, sfc–3 hPa	GCM (NCAR CCM-3)	semi-Lagrange [Williamson and Rasch, 1989]	described by Hack [1994]	O _x , NO _x , HO _x , CH ₄ , C ₂ H ₆ , C ₃ H ₈ , C ₄ H ₁₀ , C ₂ H ₄ , C ₃ H ₆ , isoprene, α -pinene	prescribed above 25 km (influx from stratosphere = 391 Tg yr ⁻¹)	12 months	Brasseur <i>et al.</i> [1998b], Hauglustaine and Brasseur [2001]

Table 2. (continued)

CTM	Institute	Contributing Authors	Domain/Resolution	Meteorology	Advection Scheme	Convection Scheme	Chemical Components	Stratospheric Ozone	Spin-Up Length	References
MOZ2	NCAR	Horowitz/ Brasseur	$2.8^\circ \times 2.8^\circ$ 34 levels, sfc—4 hPa	GCM (NCAR MACCM-3)	Lin and Rood scheme [Lin and Rood, 1996]	Zhang and McFarlane [1995] for deep convection; Hack [1994] for shallow convection	detailed ozone-NO _x - NMHC chemistry, 52 species, 150 reactions	relaxed to climatology (with 10-day time constant)	12 months	Brasseur <i>et al.</i> [1998b], Hauglustaine <i>et al.</i> [1998], L. W. Horowitz <i>et al.</i> (manuscript in preparation, 2002) Mickley <i>et al.</i> [1999]
HGIS ^b	Harvard University	Mickley/ Jacob	$4^\circ \text{lat} \times 5^\circ \text{lon}$ nine levels, sfc—10 hPa	GCM (GISS 2')	second-order moments [Prather, 1986]	described by Del Genio <i>et al.</i> [1996]	detailed ozone/NO _x / hydrocarbon scheme incl. 80 species	influx described at 150 hPa as a function of season and latitude	6 months	Mickley <i>et al.</i> [1999]
UKMO ^b	UK Met Office	Stevenson	$5^\circ \times 5^\circ$ nine levels, sfc—100 hPa	GCM (HadCM3)	Lagrangian	based on the convective precipitation rate derived from Radon-222 profiles [Stevenson <i>et al.</i> , 1998b]	detailed ozone/NO _x / hydrocarbon scheme including 70 species	influx prescribed at 100 hPa (432 Tg yr ⁻¹)	3 months	Collins <i>et al.</i> [1997], Johnson <i>et al.</i> [1999]
UIO2 ^c	University of Oslo	Gauss/ Sundet	$5.6^\circ \times 5.6^\circ$ 19 levels, sfc—10 hPa	ECMWF forecast data 1996	second-order moments [Prather, 1986]	mass flux scheme of Tiedtke [1989]	detailed ozone/NO _x / hydrocarbon scheme including 51 species, QSSA solver ^d	influx prescribed at 10 hPa (450 Tg yr ⁻¹) ^d	6 months ^a	Sundet [1997]

^aUIO2 and UIO2 perform a spin-up of 10 and 3 years, respectively, in the stratospheric experiments discussed in section 2.2.

^bThe HGIS and UKMO models reported data only up to 12 and 14 km, respectively.

^cUIO2 did not participate in OxComp. A tropospheric version of UIO2 belonging to the same CTM generation as the OxComp models is run for the analysis in this paper.

^dThe UIO2 version used for the stratospheric experiments discussed in section 2.2 applies a comprehensive stratospheric chemistry module in addition. The resulting stratospheric influx through the tropopause amounts to 686 Tg yr⁻¹.

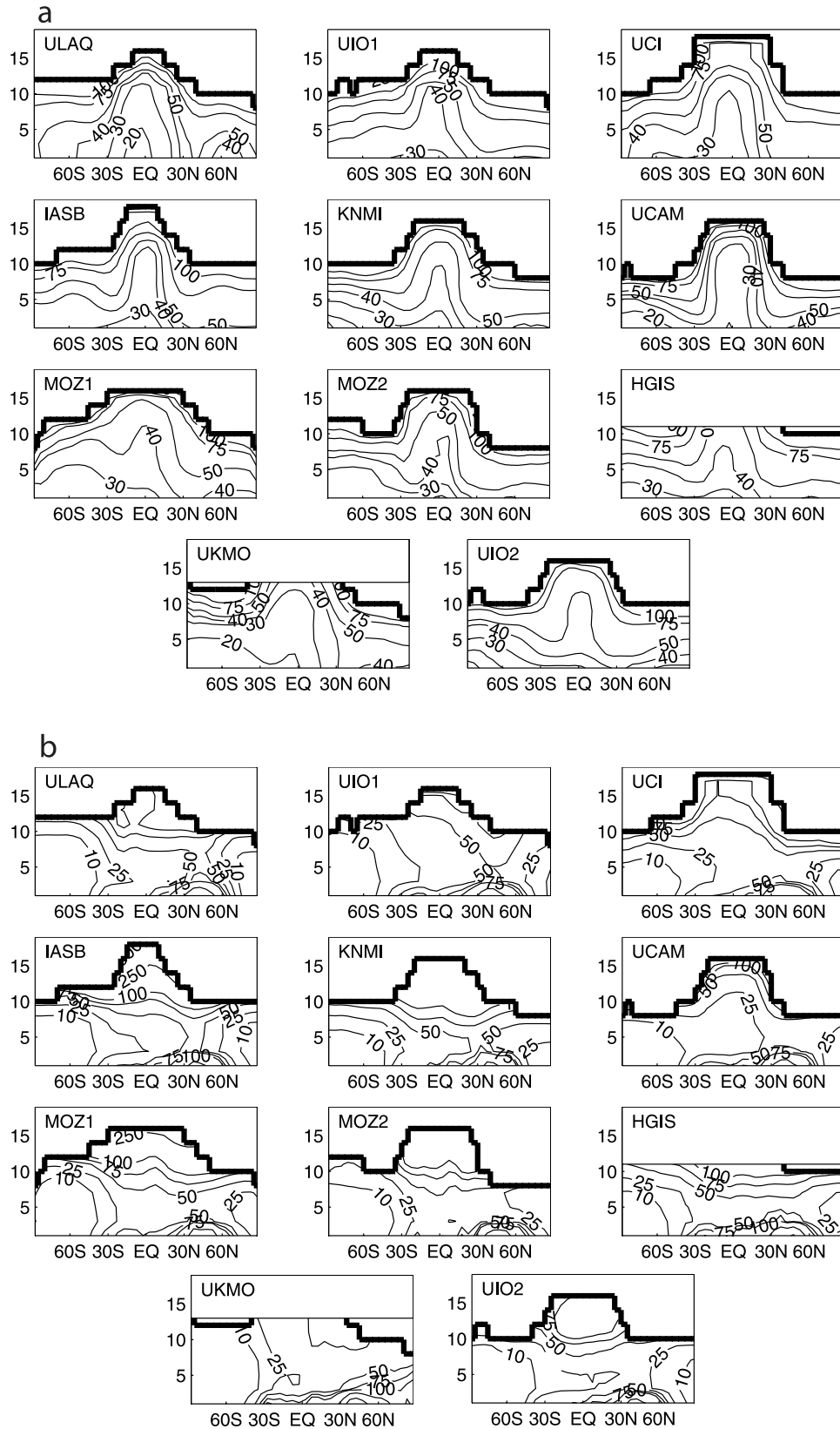


Figure 1. Annually averaged zonal mean (a) ozone and (b) NO_x modeled for the year 2000. Contour lines at 10, 20, 30, 40, 50, 75, and 100 ppbv (Figure 1a), and 10, 25, 50, 75, 100, 250, 500, and 1000 pptv (Figure 1b). As in IPCC-TAR, grid boxes with ozone mixing ratios above 150 ppbv are masked. The altitude is given in kilometers.

areas, where ozone production on a per molecule basis is more efficient. Surface mixing ratios are a maximum in midnorthern latitude to high northern latitude, amounting to 40–60 ppbv on a zonal mean. Locally, they are modeled to exceed 70 ppbv in highly polluted areas over central Europe and North America.

[21] NO_x levels are high in the lower and upper troposphere and go through a minimum at medium altitudes. An exception is in high southern latitudes where the surface maximum is absent. The clean atmosphere in these regions, characterized by NO_x levels below 10 pptv (parts per trillion by volume), is common to all models. Again, surface mixing ratios are a maximum in midnorthern latitude to high northern latitude, with a range of 200–600 pptv zonally averaged. However, in highly polluted areas they are calculated to be as high as 2–3 ppbv, depending on the model. The differences in NO_x among the models reflect the outstanding difficulty to model concentrations of NO_x in the atmosphere. High uncertainties remain, for example, in the sources of NO_x such as lightning, and in the conversion of NO_x to NO_y , as well as in the removal of HNO_3 through washout from the atmosphere. Differences in transport parameterizations in the lower troposphere, in particular boundary layer mixing and convection, will add to the uncertainty range for the short-lived NO_x components. Also, models with low horizontal resolution tend to underestimate peaks in NO_x concentration over highly polluted areas.

[22] Relatively low NO_x levels in the upper troposphere of the UCAM model are likely to be caused by too efficient rainout of HNO_3 . The very low NO_x concentrations in the UKMO upper troposphere are probably related to the convection scheme used in this model, which completely mixes in the vertical, rather than generating a C-shaped profile. Also, the relatively small downward flux of HNO_3 from the stratosphere contributes to the low NO_x levels. The relatively high NO_x values calculated by UKMO in the lower troposphere of the Northern Hemisphere are primarily due to very high wintertime levels. It is thought that these are connected with a lack of heterogeneous removal or insufficient mixing between the boundary layer and the free troposphere. Relatively high NO_x levels in this region are also modeled by HGIS, which is likely to be due to the greater biomass burning emissions used in this model (see footnote in Table 1).

[23] Changes in ozone modeled for the 21st century are displayed in Figure 2a. The calculations show that there are large differences between the models as to the spatial variation of ozone increase and to its peak magnitude. The tropospheric ozone increase varies typically between about 10 and 30 ppbv near the surface and then increases with altitude. In most models it is largest in low latitudes near the tropopause, while the increase in surface ozone peaks at about 30°N.

[24] Ozone change is caused by changes in its precursors NO_x , CO, and hydrocarbons. As an example, the calculated change of NO_x is shown in Figure 2b, explaining in part the differences in modeled ozone change. NO_x increases are largest at the surface, amounting to several hundred pptv in midnorthern latitudes, and then decrease with height. MOZ1 and IASB calculate even a slight decrease in NO_x in the upper troposphere, which is partly due to a more efficient conversion from NO_x to HNO_3 caused by comparatively

high OH levels in these altitudes calculated by these models. Furthermore, IASB calculates NO_x species in the stratosphere from the vertical gradient within the domain below, where chemistry is integrated. This method might lead to artifacts in the modeled stratospheric response to emission changes in this model.

[25] In most other models, the NO_x increase starts to rise again above a certain level in the middle troposphere. Differences in the applied convection schemes partly explain the spread in modeled NO_x increase. For instance, in MOZ2 the increase in NO_x in the upper tropical tropopause is much larger than in MOZ1. This is due in part to the significantly different treatment of convection in MOZ1 and MOZ2. MOZ1 parameterizes shallow convection based on the scheme of Hack [1994], but does not get strong deep convection. The large surface NO_x emissions are thus not communicated efficiently to the upper troposphere. In MOZ2, on the other hand, the Zhang and McFarlane [1995] scheme is used for deep convection (in addition to the Hack scheme for shallow convection) allowing short-lived NO_x species to be transported rapidly to the upper troposphere. Similarly, the large NO_x increase in the UIO1 upper tropical troposphere results from a relatively strong convective transport in UIO1, which was already identified by Berntsen and Isaksen [1999].

[26] The positive correlation between increases in NO_x and ozone is clearly revealed, especially in the upper troposphere. Models that calculate a relatively high NO_x increase in this region (UIO1, UCI, MOZ2, and HGIS) yield a correspondingly high ozone increase. Regarding the seasonal variation, largest increases in ozone are modeled in the tropopause region in northern midlatitudes during Northern Hemisphere summer, reflecting the location of maximum increases in emissions and maximum availability of sunlight.

[27] All models calculate a CO enhancement (not shown) from increasing fossil fuel burning, with peak relative increases showing up in low latitudes. ULAQ, KNMI, MOZ1, and HGIS obtain increases of up to 150% in the equatorial troposphere. CO has a lifetime of about 1.5 months in the troposphere, i.e., much longer than the lifetime of NO_x , which explains why the calculated increase is pronounced throughout the troposphere.

[28] For the calculation of the tropospheric ozone column changes displayed in Figure 3 the same tropopause definition was used for each model. It is based on the temperature gradient as described by Berntsen *et al.* [1997] and is applied in the radiative forcing calculations to be discussed in section 3.

[29] Two belts of enhancement are seen along the tropics, strongly emphasizing the role of zonal transport from polluted regions. Relatively large increases still occur over remote areas such as the northern and southern Pacific and southern Indian Ocean. The models generally predict large increases along the southern edge of Asia from Arabia to eastern China. Common to most models are large increases in low latitudes, related to high levels of ozone precursors and sunlight, but also reflecting the greater thickness of the troposphere in the tropics. Maximum increases are modeled over Southern Asia, especially over India and the southeastern part of China, while increases are generally low over

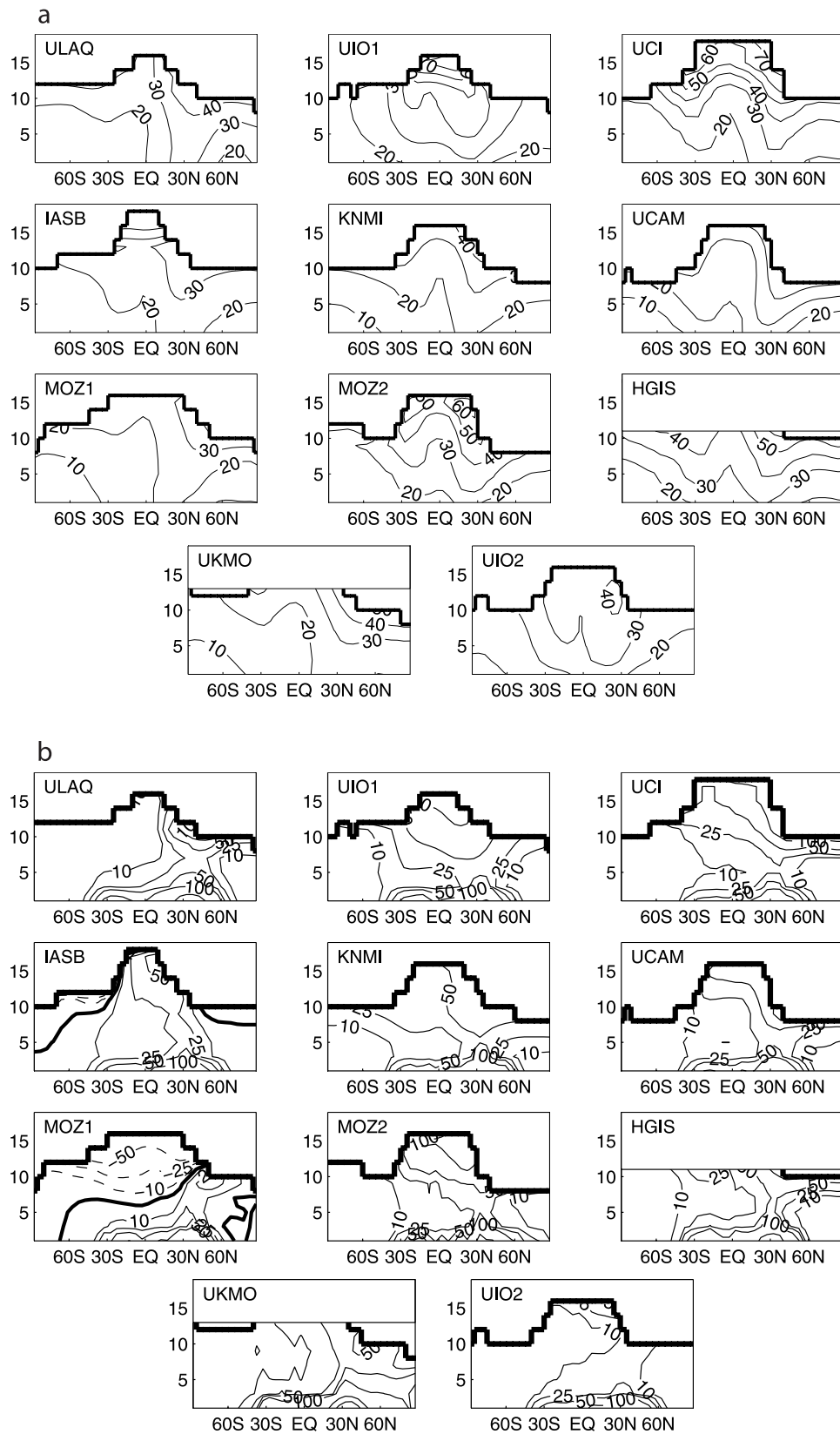


Figure 2. Increase in annually averaged zonal mean (a) ozone and (b) NO_x between 2000 and 2100 (year 2100 values minus year 2000 values). All models in this figure used fixed ozone levels, ozone flux, or ozone precursor levels in the stratosphere. Contour lines at 10, 20, 30, 40, 50, 60, 70, and 80 ppbv (Figure 2a), and at -100, -50, -25, 0, 10, 25, 50, 100, 250, 500, and 1000 pptv (Figure 2b) (negative contour lines dashed). As in IPCC-TAR, grid boxes with (year 2000) ozone mixing ratios above 150 ppbv are masked. The altitude is given in kilometers.

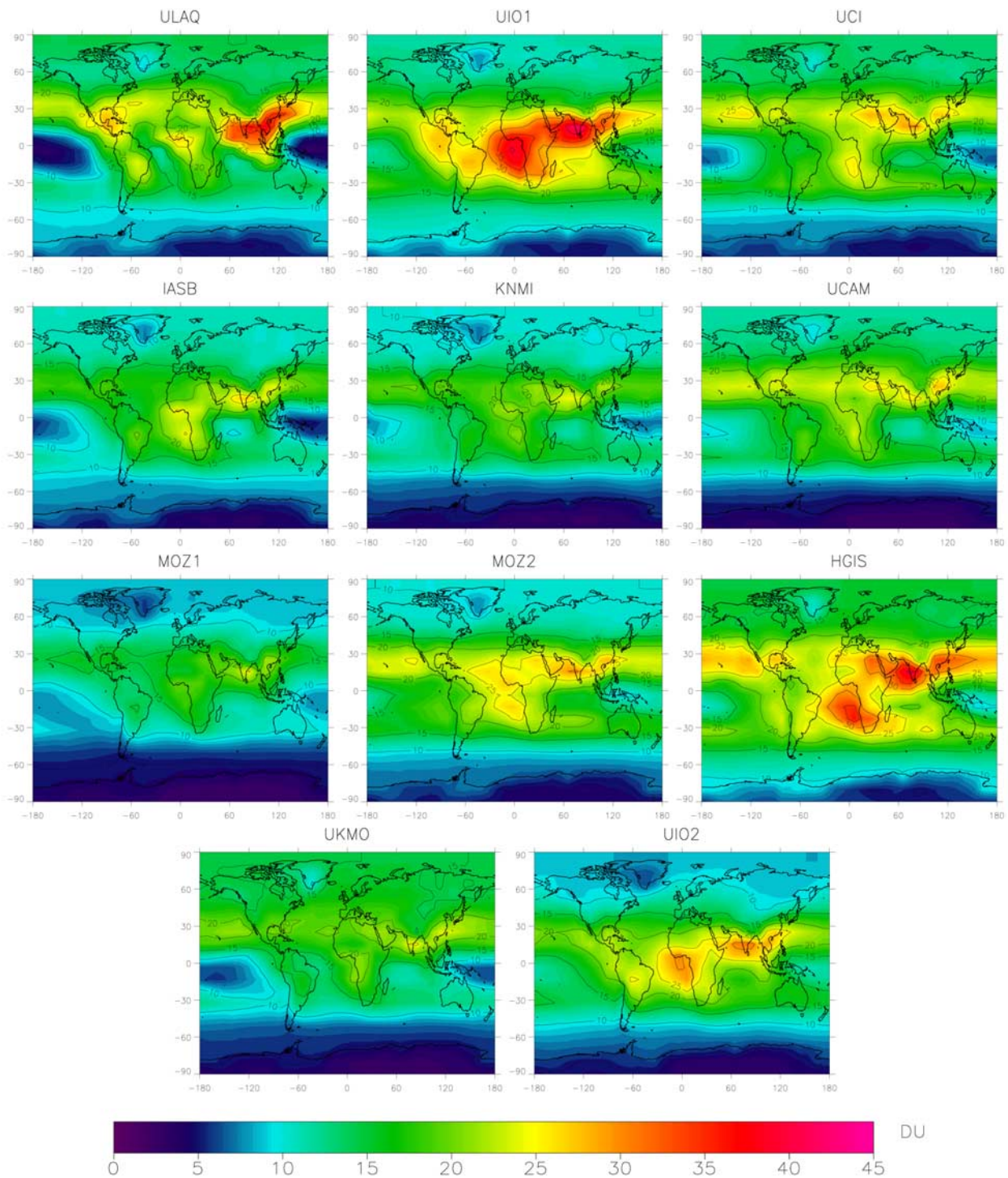


Figure 3. Change in the annual mean tropospheric ozone column from 2000 to 2100 (DU). The tropopause level in this calculation is based on the temperature gradient as described by *Berntsen et al.* [1997].

remote marine areas and in high latitudes, decreasing to almost zero over the Antarctic continent. The relatively small ozone increases over Antarctica and Greenland are due to the relatively small increase of ozone precursors and to the high surface elevation (reducing the height of the troposphere).

[30] Most models yield a secondary maximum over the tropical Atlantic Ocean, in particular near the African coast. *Fishman et al.* [1996] attribute the large sensitivity of ozone in this region to transport of precursors from widespread biomass burning on the adjacent continents and to the meteorology, which is favorable for the accumulation of

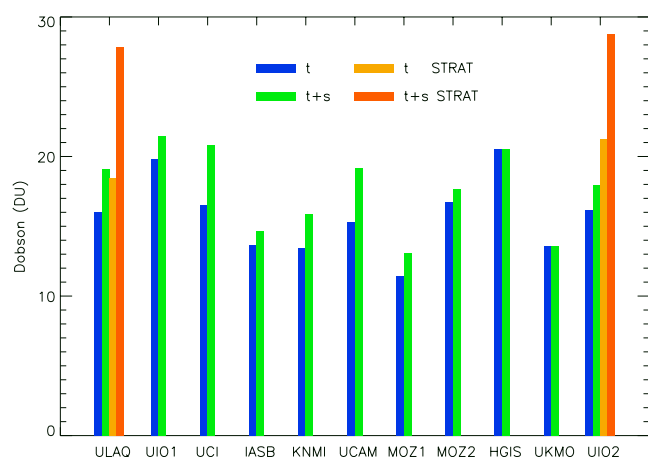


Figure 4. Change in the annual mean globally averaged ozone column from 2000 to 2100 (DU). t, troposphere only; t + s, troposphere + lower stratosphere (up to 20 km). The orange and red bars show results from the two simulations that calculated stratospheric change explicitly (see section 2.2). The tropopause level in this calculation was based on the temperature gradient as described by *Bernsten et al.* [1997].

ozone precursors over the tropical Atlantic basin. Differences in horizontal transport as well as different parameterizations of washout and convection also explain the large differences over the West Pacific in low northern latitudes.

[31] The largest peak values are generated by ULAQ, UIO1, and HGIS. While ozone increases in these models are relatively high over the whole globe, the horizontal gradients found between low and midlatitudes are larger compared with, for instance, UKMO, MOZ1, and KNMI. Reasons for this might be related with large-scale transport of ozone precursors, chemistry, and convection. Strong convection tends to enhance column ozone in polluted areas through more efficient processing of ozone precursors, while it reduces column ozone in clean areas. UKMO has a relatively weak convection, hence ozone production efficiency from NO_x over polluted areas is reduced. Also, its NMHC chemistry tends to generate high levels of PAN, thus enabling long-range horizontal transport of NO_x . Both of these factors favor relatively low horizontal gradients in ozone. Less vigorous convection also explains the smaller ozone change in KNMI. By contrast, HGIS calculates a more vigorous convection leading to a bigger ozone change as compared to other models despite a similar NO_x change over low latitudes. Similarly, the deep convection scheme included in MOZ2 probably explains its larger peaks in ozone increase compared with MOZ1, which accounts for shallow convection only. ULAQ has a rather weak horizontal transport in the lower troposphere as was recently discussed for the case of aerosols by *Kinne et al.* [2003]. Differences between sources and remote regions can thus be rather strong in the ULAQ model.

[32] Figure 4 shows the increase in the global annual mean ozone column calculated for the 21st century. The change in globally integrated tropospheric ozone is positive in all models ranging from +11.4 DU (MOZ1) to +20.5 DU (HGIS). In the model calculations that applied the fixed

stratosphere approach (see above) any stratospheric ozone change is largely due to transport effects (with the increase of tropospheric ozone propagating into the lower stratosphere), and to a minor degree to deviating tropopause definitions in the respective models (in the present analysis the same tropopause was applied to all data sets implying that the stratospheric contribution may in some cases contain parts of the models' upper troposphere). Variations among the calculated stratospheric changes are mainly due to the different methods of forcing stratospheric chemistry to year 2000 conditions (discussed above).

2.2. Additional CTM Experiments Including Stratospheric Change

[33] One obvious gap in the above projections is the omission of stratospheric changes to be expected for the 21st century. The stratospheric ozone layer is assumed to recover during the next decades following the decrease of chlorine and bromine levels [*WMO*, 1999]. Another important impact on the stratosphere is the response to increases in CH_4 and N_2O projected by most scenarios [*Hofmann and Pyle*, 1999]. Through interactions with both shortwave and longwave radiation, changes in stratospheric ozone imply a direct impact on radiative forcing. Tropospheric chemistry will also be influenced by ozone changes in the stratosphere through changes in shortwave radiation. The depletion that has been observed over the past three decades has led to increases in tropospheric UV and is assumed to have increased the oxidizing capacity of the troposphere by forcing tropospheric OH abundances upward [*Bekki et al.*, 1994; *Fuglestedt et al.*, 1994]. Ozone depletion may also have reduced the influx of ozone from the stratosphere, which would reduce tropospheric ozone [*Karlsdottir et al.*, 2000] and tend to reverse the OH trends. *Prinn et al.* [2001] present observational evidence that OH levels have declined during the last decade.

[34] In a future atmosphere characterized by increasing stratospheric ozone levels the effects of increasing UV levels would be reversed. In order to study the combined effect of future tropospheric and stratospheric changes the ULAQ and UIO2 models are applied with both tropospheric and stratospheric chemistry in an additional experiment, where the stratosphere is allowed to adjust freely to 2100 conditions responding to changing emissions and tropospheric abundances. However, as in the tropospheric calculations of section 2.1, the meteorology is the same for the 2000 and 2100 simulations, i.e., no climatic change is taken into account. ULAQ uses GCM meteorology characteristic of year 2000 conditions, while UIO2 applies ECMWF reanalysis data for the year 1996. In order to obtain stable results for stratospheric perturbations the spin-up time was increased considerably with respect to the tropospheric experiments (see Table 2). For each year the same set of meteorological data is used.

2.2.1. Description of the ULAQ and UIO2 Experiments

[35] The ULAQ model extends from the surface up to the midmesosphere and its chemical scheme includes all families relevant to stratospheric ozone photochemistry (NO_x , HO_x , CHO_x , ClO_x , BrO_x , O_x) as well as the most relevant hydrocarbon chemistry for the troposphere and heterogeneous reactions in the stratosphere. Owing to these features the model is particularly suitable for the calculation of the

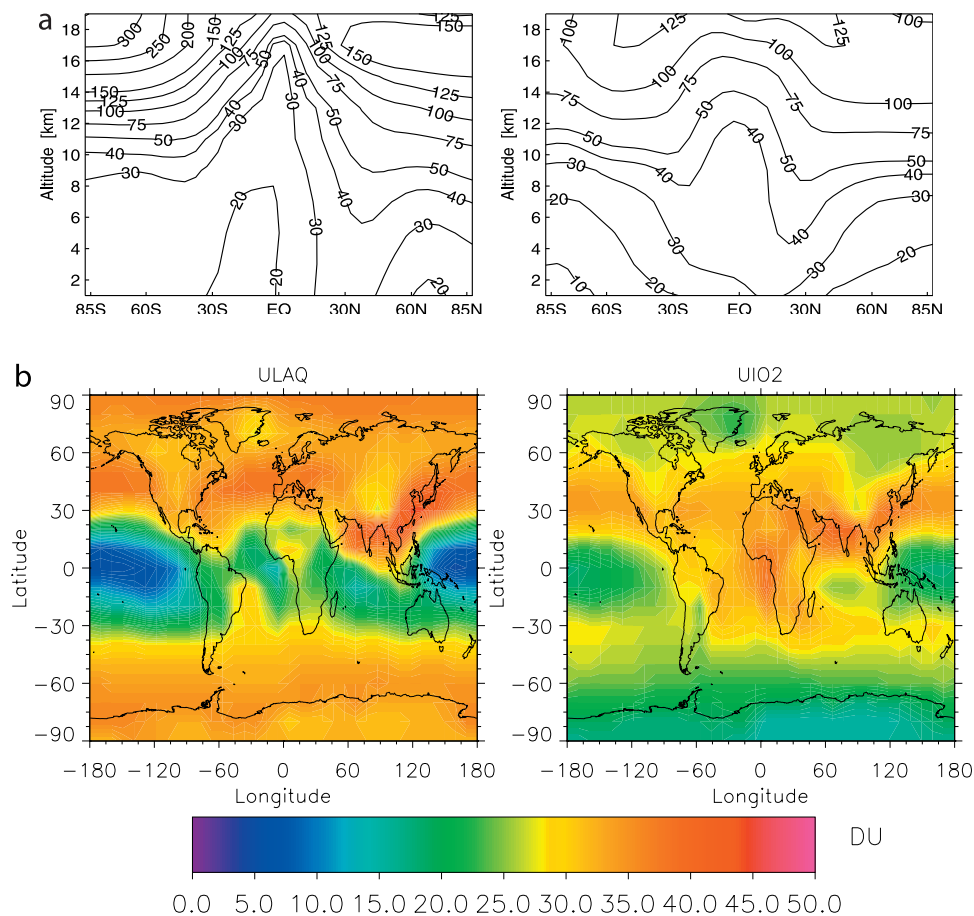


Figure 5. Change in ozone between 2000 and 2100 calculated by ULAQ (first panels) and UIO2 (second panels), when taking into account stratospheric changes. (a) Change in annually averaged zonal mean ozone (ppbv), and (b) change in the annual mean ozone column integrated from the surface up to 20 km (DU).

large secular ozone trends to be expected for the 21st century. For the ULAQ simulations reported in section 2.1, this model used the fixed stratosphere approach of OxComp by applying the year 2000 specifications for CFCs and HCFCs and by adjusting the N_2O and CH_4 mixing ratios to the previously stored 2000 values above the online calculated 200 ppbv ozone level. By contrast, in this additional experiment we specify CFCs and HCFCs in the troposphere according to *WMO* [1999] recommended values for 2100. As listed in Table 1, tropospheric N_2O and CH_4 are set equal to 455 and 4300 ppbv, respectively, and are left to respond naturally above the 200 ppbv ozone level.

[36] In the second experiment a new version of the UIO2 model is applied, including two comprehensive chemistry schemes, one for the troposphere [Berntsen and Isaksen, 1997] and the other for the stratosphere [Rummukainen *et al.*, 1999]. Apart from that the model framework is identical to the UIO2 version used for the experiment described in section 2.1 (see Table 2). Heterogeneous chemistry on aerosols and polar stratospheric clouds is calculated using the microphysical module of *Carslaw et al.* [1995]. As in the ULAQ experiment, tropospheric levels of CFCs, HCFCs, N_2O , and CH_4 for the year 2100 are implemented according to Table 1. The stratospheric chemistry module is applied above the 150 ppbv (year 2000) ozone level, and

calculates the response of stratospheric concentrations to the changing emissions.

2.2.2. Results

[37] Results for the global mean ozone column change (up to 20 km) calculated by both models in this experiment are included in Figure 4 (orange and red bars). The two models agree rather well, yielding values of 27.8 and 28.7 DU, respectively, for the troposphere and stratosphere combined. The stratospheric ozone increase, visualized by the difference between the orange and red bars, is significantly larger than in the runs based on the fixed stratosphere approach used in OxComp. The additional ozone in the lower stratosphere implies a further increase in ozone also in the troposphere due to an increased downward flux into the troposphere. The tropospheric ozone change (orange bars) calculated by ULAQ now amounts to 18.5 DU on a global and annual mean, while UIO2 predicts 21.2 DU. These values are larger than those indicated by the blue bars in Figure 4, which refer to the runs with a fixed stratosphere approach yielding 16.0 and 16.2 DU for ULAQ and UIO2, respectively.

[38] Annual mean changes in zonal mean ozone and horizontal maps of changes in the ozone column up to 20 km are displayed in Figure 5 and should be compared to the results shown in Figures 2 and 3 that display tropospheric

changes only. The ULAQ model calculates maximum ozone increase in high latitudes, especially over the Southern Hemisphere exceeding 300 ppbv at around 20 km altitude, while UIO2 yields a less pronounced ozone recovery with a maximum around 130 ppbv in low and midlatitudes and 20 km altitude. Regarding the stratosphere, better agreement between the models is seen over the Arctic, with an increase of around 160 ppbv for ULAQ and 120 ppbv for UIO2. The increase in the ozone column is substantial also in midlatitudes and high latitudes, although the maximum is still situated in low latitudes over the Far East where ozone increases exceed 45 and 35 DU in the ULAQ and UIO2 models, respectively. A comparison with the corresponding panels in Figure 3 reveals that the stratospheric contribution to the ozone column increase is greatest in high latitudes. The reason for the disagreement between ULAQ and UIO2 at high altitudes over the Antarctic is mainly due to chlorine- and bromine-induced ozone depletion, which plays a larger role in ULAQ, resulting in a deeper ozone hole and a more pronounced recovery during the 21st century as compared to the UIO2 calculation. However, it must be stressed that both the ULAQ and the UIO2 models underestimate the ozone depletion over the Antarctic in comparison with satellite- and ground-based observations [e.g., *De Winter-Sorkina*, 2001; *McPeters et al.*, 1996; *WMO*, 1999]. UIO2, which uses meteorology for the year 1996, has been thoroughly validated against “GOME” satellite data over the Antarctic and overestimates the total ozone column by almost 30% during the Antarctic spring. This points to problems in heterogeneous chemistry involving chlorine and bromine species, and in the parameterization of microphysical processes (e.g., denitrification). Due to the weaker ozone depletion in the models the ozone recovery rate is probably underestimated as well. In the context of this paper this suggests that the radiative forcing due to stratospheric ozone increases in the 21st century is likely to be larger than indicated by the results in section 3. However, this consideration does not take into account the uncertainties related to climate change, which will be further discussed in the section 4.

2.2.3. NO_x and Ozone Precursor Changes Versus Decreasing Chlorine and Bromine Levels

[39] The modeled increase in ozone in the lower stratosphere is a result of (1) enhanced levels of NO_x and ozone precursors that were the subject of chapter 4 in IPCC-TAR and (2) the decrease in chlorine and bromine levels following the Montreal protocol and its amendments. By the year 2100 levels of total chlorine and bromine in the atmosphere are expected to have decreased substantially [*WMO*, 1999], while NO_x in the lower stratosphere will increase further as a result of higher N₂O influx from the troposphere. The role of NO_x increases in the chemistry of ozone is highly dependent on altitude [see, e.g., *Brasseur et al.*, 1998c]. Additional NO_x in the lower atmosphere will induce an ozone increase through the CO oxidation chain, while at higher altitudes NO_x promotes an important catalytic ozone depletion cycle. On the other hand, it leads to diminished ozone loss by chlorine, bromine, and odd hydrogen catalytic cycles in the lower stratosphere [*Wennberg et al.*, 1994].

[40] In order to estimate the individual contributions of the chlorine/bromine and the NO_x effects, the 2100 experiment is repeated with the UIO2 model keeping chlorine and

bromine levels at their year 2000 levels. In this new simulation the globally and annually averaged increase in the ozone column (up to 20 km) amounts to 25.0 DU, which is less than the 28.7 DU obtained in the experiment that includes chlorine and bromine decreases (section 2.2.2). The stratospheric contribution amounts to 5.0 DU, compared to 7.5 DU in the experiment of section 2.2.2. Although the chlorine/bromine and the NO_x effects are not independent of each other, it can be concluded that the increases in NO_x and ozone precursors contribute substantially to the calculated increase in lower stratospheric ozone.

2.3. Conclusions of the CTM Study

[41] Both the OxComp study and the additional stratospheric study conducted for this paper point to the rather high uncertainty regarding the spatial pattern of ozone change. Yet the simulated change of the globally and annually averaged tropospheric ozone column seems to be rather robust and lies within the range of 11.4–20.5 DU. The similarity in the total, but difference in the location, of the predicted ozone increases was already noted by *Isaksen and Jackman* [1999] and is probably due to the different meteorological data sets used in the models as well as the different transport formulations as was documented in previous CTM intercomparisons [*Jacob et al.*, 1997]. For example, convection is represented in all CTMs, but in quite different ways, and it involves parameterization of processes occurring on a subgrid scale. Convection affects the NO_x and HO_x budgets and thereby photochemical ozone production significantly in the upper troposphere [e.g., *Prather and Jacob*, 1997; *Collins et al.*, 1999; *Müller and Brasseur*, 1999]. Furthermore, convection leads to enhanced downward transport of ozone into regions where it has a shorter lifetime [*Lelieveld and Crutzen*, 1994; *Berntsen and Isaksen*, 1999]. Another source of differences between the models is boundary layer transport, which is parameterized in different ways and affects short-lived gases such as NO_x, thus further modifying the effect of changing emissions on ozone, particularly in the lower troposphere. More specifically, a further improvement of consistency among the models would require a higher horizontal resolution but also a much more detailed database on NO_x emissions from sources with small-scale variability such as biomass burning and lightning emissions. The better agreement on the averaged ozone increase may reflect a more uniform ozone production as a function of NO_x emissions and methane abundances on a global scale. In other words, nonlinearities in the ozone-NO_x chemical system, albeit of great local importance in polluted areas, seem to have less impact when global averages are considered. However, as shown in the next section the large model range in the predicted patterns of ozone perturbations leads to a larger uncertainty in local climate impact than Figure 4 might suggest. Also, it has to be kept in mind that the A2p emission scenario used here is only one of several scenarios derived by SRES. Thus the uncertainty range given here reflects only the uncertainty of chemical transport modeling, while the consideration of further emission uncertainties would result in a larger uncertainty range. As the A2p scenario constitutes the worst case proposed in IPCC-TAR, the results presented here may be considered as an upper limit.

[42] Concerning the lower stratosphere it is clear that increases of ozone will be important for radiative forcing in the 21st century, although the model uncertainties with respect to the details of ozone recovery are still large.

[43] The following section will present radiative forcing calculations both for tropospheric increases only and for changes in the troposphere and the lower stratosphere combined.

3. Radiative Transfer Calculations

[44] The radiative transfer schemes for thermal infrared radiation and solar radiation used in this study are the same as in the work of *Berntsen et al.* [1997], *Berntsen and Isaksen* [1999], and *Myhre et al.* [2000]. The thermal infrared scheme is an absorptivity/emissivity broadband model and the solar scheme is a multistream model using the discrete ordinate method (for more details see *Myhre et al.* [2000]). Temperature, water vapor, and surface albedo are taken from the ECMWF and cloud data from the ISCCP as in the above mentioned papers. The tropopause level is based on the temperature gradient as described by *Berntsen et al.* [1997] and is the same for all radiative forcing calculations in order to allow a convenient standardization between models. For “radiative forcing” we follow the definition of IPCC-TAR chapter 6 [*Ramaswamy et al.*, 2001], which includes the stratospheric temperature adjustment. Calculations where the stratospheric temperature adjustment is excluded are denoted as “instantaneous radiative forcing.”

3.1. Radiative Forcing Due to Tropospheric Ozone Change

[45] Figure 6 shows the annual mean radiative forcing due to changes in tropospheric ozone between 2000 and 2100 as calculated in the experiments focusing on changes in the troposphere only. It has to be stressed here that stratospheric changes from these model calculations are not used in these radiative transfer calculations, i.e., their contribution to radiative forcing will be limited by their influence on ozone levels in the troposphere through transport processes. Global mean net radiative forcing values are listed in Table 3 and will be discussed in the end of this section.

[46] Large differences can be seen in the magnitude of the forcing, whereas the geographical pattern is more similar. Also, the models agree rather well on the pattern of radiative forcing divided by the maximum radiative forcing. A high radiative forcing is calculated in the region around 20°N with a large zonal extent and a maximum over the Sahara or the Arabian desert. A second, more zonally confined maximum is calculated around 20°S. The maximum radiative forcing around 20°S is west of southern Africa, with a secondary maximum west of South America. A common feature is that the forcing is low over the Pacific Ocean near the equator, especially in the western Pacific Ocean. Furthermore, the forcing is low in all the models southward of 60°S, with values generally below 10% of the maximum forcing. Northward of 30°–40°N there are somewhat larger differences between the models, illustrated by the contrast between the forcing modeled in this region and the respective maximum forcings found in low latitudes. In the UIO1,

MOZ2, and UIO2 models this contrast is relatively large, whereas in the case of UKMO it is much smaller. Compared with radiative forcing due to changes in tropospheric ozone since the preindustrial era, which has been estimated by several studies [*Ramaswamy et al.*, 2001], the pattern of future radiative forcing exhibits a relatively larger forcing in the tropical region.

[47] When judging the correlation between column ozone change displayed in Figure 3 and radiative forcing in Figure 6 it has to be kept in mind that radiative forcing depends strongly on the vertical distribution of the modeled ozone change. Differences with respect to the height distribution of ozone change will thus add to the differences between the horizontal patterns in Figures 3 and 6.

[48] Therefore we display in Figure 7, the modeled annual mean normalized radiative forcing (radiative forcing divided by the ozone column change) [*Haywood et al.*, 1998; *Berntsen et al.*, 2000], which is a useful tool for investigation of radiative effects of ozone changes. The 11 models show very similar patterns with high values from 30°N to 30°S and a maximum over the Sahara or the Pacific Ocean. Differences in normalized radiative forcing are mainly due to differences in the altitude of ozone change, and to a much lesser extent, in the background levels of tropospheric ozone, connected with a slight saturation effect as discussed by *Berntsen et al.* [2000]. The normalized radiative forcing calculations from the 11 models have many similarities to a simulation that was done by *Berntsen et al.* [1997] with a 10 ppbv increase in the tropospheric ozone mixing ratio.

[49] To further understand the differences in normalized radiative forcing we show in Figure 8 global and annual mean longwave, shortwave, and net normalized radiative forcing components for clear and cloudy conditions. The results are consistent with the discussion in the work of *Berntsen et al.* [1997] where it is shown that the longwave forcing dominates the shortwave forcing due to ozone and that clouds reduce the longwave radiative forcing and increase the shortwave forcing. The net effect of clouds is generally to decrease the radiative forcing, but varies between different models [*Roelofs*, 1999]. Furthermore, stratospheric temperature adjustment reduces the longwave radiative forcing (see discussion of *Berntsen et al.* [1997]).

[50] The shortwave component of clear-sky normalized radiative forcing shows little variation among the 11 models, lying within 12%. Similarly, the results when clouds are included vary by less than 15%. The main reason for these variations is the different geographical distribution of the ozone change, the shortwave radiative forcing due to tropospheric ozone changes being larger over surfaces with high albedo than over those with low albedo. Therefore both the spatial pattern and the altitude of the ozone change are important when clouds are included. The shortwave normalized radiative forcing when clouds are included is between 42 and 52% higher than for the clear-sky case.

[51] The normalized instantaneous longwave radiative forcing under clear-sky conditions has a variation of 20% among the 11 models. The most important reason for this variation is not only the differences in the altitude of the calculated ozone change, but also its geographical distribution and the different ozone levels calculated for the year 2000. When clouds are included the models with the lowest

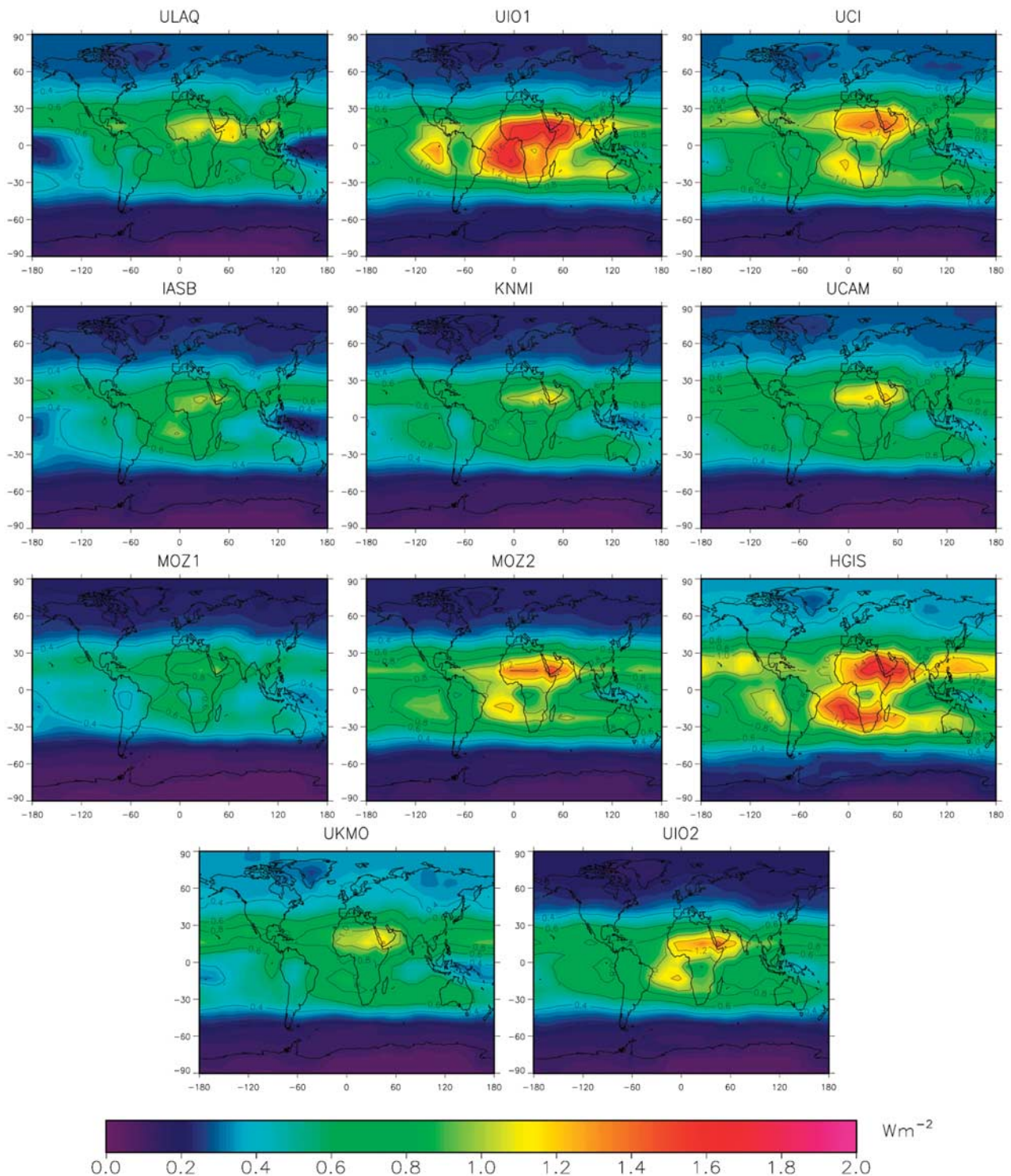


Figure 6. Radiative forcing (W m^{-2}) between 2000 and 2100 taking into account ozone changes in the troposphere only (i.e., up to the tropopause level based on the definition of *Berntsen et al.* [1997]). All models in this figure used fixed ozone levels, ozone flux, or ozone precursor levels in the stratosphere.

normalized instantaneous clear-sky longwave radiative forcing are most influenced by the clouds. This is because ozone changes below clouds will give a very small radiative forcing and the models with the lowest normalized instantaneous clear-sky longwave radiative forcing generally calcu-

late the ozone change at a lower altitude as compared to the other models. With stratospheric temperature adjustment included, all the models have a reduced normalized radiative forcing, but the magnitude depends on a complex combination of the altitude of ozone change, the geograph-

Table 3. Radiative Transfer Calculations Based on Modeled Tropospheric Ozone Changes^a

Model	ΔO_3 , DU	SW RF, $W m^{-2}$	LW RF, $W m^{-2}$	RF, $W m^{-2}$	RF (NH/SH)	NRF, $W m^{-2}$ DU ⁻¹	NRF (NH/SH)
ULAQ	16.0	0.15	0.36	0.51	1.51	0.032	0.96
UIO1	19.8	0.20	0.50	0.70	1.15	0.035	0.98
UCI	16.5	0.18	0.48	0.66	1.26	0.040	0.93
IASB	13.7	0.13	0.31	0.44	1.32	0.032	0.97
KNMI	13.4	0.14	0.34	0.47	1.28	0.035	0.94
UCAM	15.3	0.16	0.38	0.53	1.45	0.035	0.95
MOZ1	11.4	0.11	0.29	0.40	1.39	0.035	0.92
MOZ2	16.7	0.17	0.44	0.62	1.21	0.037	0.92
HGIS ^b	20.5	0.22	0.56	0.78	1.18	0.038	0.96
UKMO ^b	13.6	0.14	0.39	0.53	1.50	0.039	0.88
UIO2	16.2	0.16	0.40	0.56	1.21	0.034	0.98
Mean	15.7	0.16	0.40	0.56	1.31	0.036	0.94
Std. dev.	2.74	0.03	0.08	0.12	0.13	0.003	0.03

^a ΔO_3 , tropospheric ozone change; SW RF, shortwave radiative forcing; LW RF, longwave radiative forcing; RF, net radiative forcing; RF (NH/SH), ratio between radiative forcing in the Northern Hemisphere to radiative forcing in the Southern Hemisphere, NRF, normalized radiative forcing (all values are annually and globally averaged).

^bAssuming zero change in the tropical troposphere above the upper boundary of the model gives 18.7 DU ozone change and a radiative forcing of 0.63 $W m^{-2}$ for HGIS, while for UKMO we obtain 13.0 DU ozone change and a radiative forcing of 0.48 $W m^{-2}$.

ical distribution of the ozone change and the background ozone level. The variation among the 11 models for the normalized longwave radiative forcing amounts to almost 30%. Clouds and stratospheric temperature adjustment reduce the longwave normalized radiative forcing by 41–47% for the 11 models.

[52] As far as the seasonal variation in global mean radiative forcing due to changes in tropospheric ozone from 2000 to 2100 is concerned, all models show a maximum during summer. For the MOZ1 model values between 0.33 $W m^{-2}$ in January and 0.48 $W m^{-2}$ in August are obtained, while HGIS has its minimum (0.72 $W m^{-2}$) in February and maximum (0.85 $W m^{-2}$) in August. MOZ1 and HGIS bound all other models in all months. To further analyze the seasonal variation we normalize for each model the global mean radiative forcing by the annual average. The agreement between the models is very good (within 10% for each month), except for UCAM, which calculates a larger seasonal variation. This is mainly due to a larger seasonal variation in the magnitude of the ozone change.

[53] Table 3 summarizes the global and annual mean results for the tropospheric ozone change from 2000 to 2100. Globally and annually averaged, the radiative forcing ranges from 0.40 to 0.78 $W m^{-2}$. The ozone change and the corresponding radiative forcing from 2000 to 2100 are higher than for the period from preindustrial to present [Ramaswamy *et al.*, 2001]. All models in the intercomparison yield a larger radiative forcing in the Northern Hemisphere than in the Southern Hemisphere but the range among the models is relatively large. The radiative forcing in the Northern Hemisphere is calculated to be 15–51% larger than the radiative forcing in the Southern Hemisphere. The normalized radiative forcing ranges from 0.032 to 0.040 $W m^{-2} DU^{-1}$ among the 11 models. In IPCC [Ramaswamy *et al.*, 2001] a comparison was made for models calculating the radiative forcing for ozone change

from preindustrial to present time with a range in the normalized radiative forcing from 0.033 to 0.056 $W m^{-2} DU^{-1}$ and a mean of 0.042 $W m^{-2} DU^{-1}$. In all radiative transfer calculations of the present study we use the same radiative transfer codes and the same meteorological data, i.e., only the calculated ozone changes differ between the calculations. In two papers of *Berntsen et al.* [1997, 2000] the UIO1 model was used along with the same radiative transfer schemes and meteorological data as in this study. For ozone changes from preindustrial to present time the two studies obtained a normalized radiative forcing of 0.041 and 0.036 $W m^{-2} DU^{-1}$, respectively. In the present study the normalized radiative forcing for UIO1 is slightly smaller (0.035 $W m^{-2} DU^{-1}$), but factors such as larger background ozone abundance and a different geographical distribution of the ozone changes influence the result. The normalized radiative forcing is modeled to be larger in the Southern Hemisphere than in the Northern Hemisphere, which is mainly due to smaller background ozone abundance and a larger fraction of the ozone change in tropical regions.

[54] Since the two models, HGIS and UKMO, did not report results for the upper tropical troposphere, two separate calculations are made for each of these models: The first one keeps the relative change in the upper tropical troposphere constant and equal to the relative change in the top level of the model, while the second one assumes zero change above the top level reported by the model. Results of the first calculation are listed in Table 3, while the results of the second calculation are mentioned in the footnote of Table 3. The assumption of zero change above the model top leads, in particular, to a reduced longwave radiative forcing and thereby to a smaller net radiative forcing and to a smaller normalized radiative forcing.

3.2. Radiative Forcing Due to Stratospheric Ozone Change

[55] As was shown in Figure 4, all CTMs calculate a global and annual mean increase in ozone in the lower stratosphere, with largest change predicted by the two models including stratospheric chemistry.

[56] The shortwave, longwave, and net radiative forcing for ozone changes strictly in the troposphere and ozone changes both in the troposphere and stratosphere are shown in Figure 9. An increase in ozone in the stratosphere allows less solar radiation to penetrate to the surface/troposphere system giving a negative shortwave radiative forcing. An increase in ozone results in a positive longwave radiative forcing being especially large for ozone changes near the tropopause [Hansen *et al.*, 1997; Forster and Shine, 1997]. The longwave radiative forcing dominates the shortwave radiative forcing for ozone changes in the lower stratosphere, so all models yield an additional positive radiative forcing due to the increase in ozone in the lower stratosphere. By taking the ozone change in the lower stratosphere into account the global and annual mean radiative forcing averaged among models without explicit calculation of stratospheric change increases from 0.56 to 0.62 $W m^{-2}$. For the models calculating stratospheric changes (ULAQ and UIO2) this number increases from 0.66 to 0.82 $W m^{-2}$, as shown in Table 4, which summarizes the results for these two experiments. For the additional UIO2 experiment for 2100 without changes in chlorine and bromine

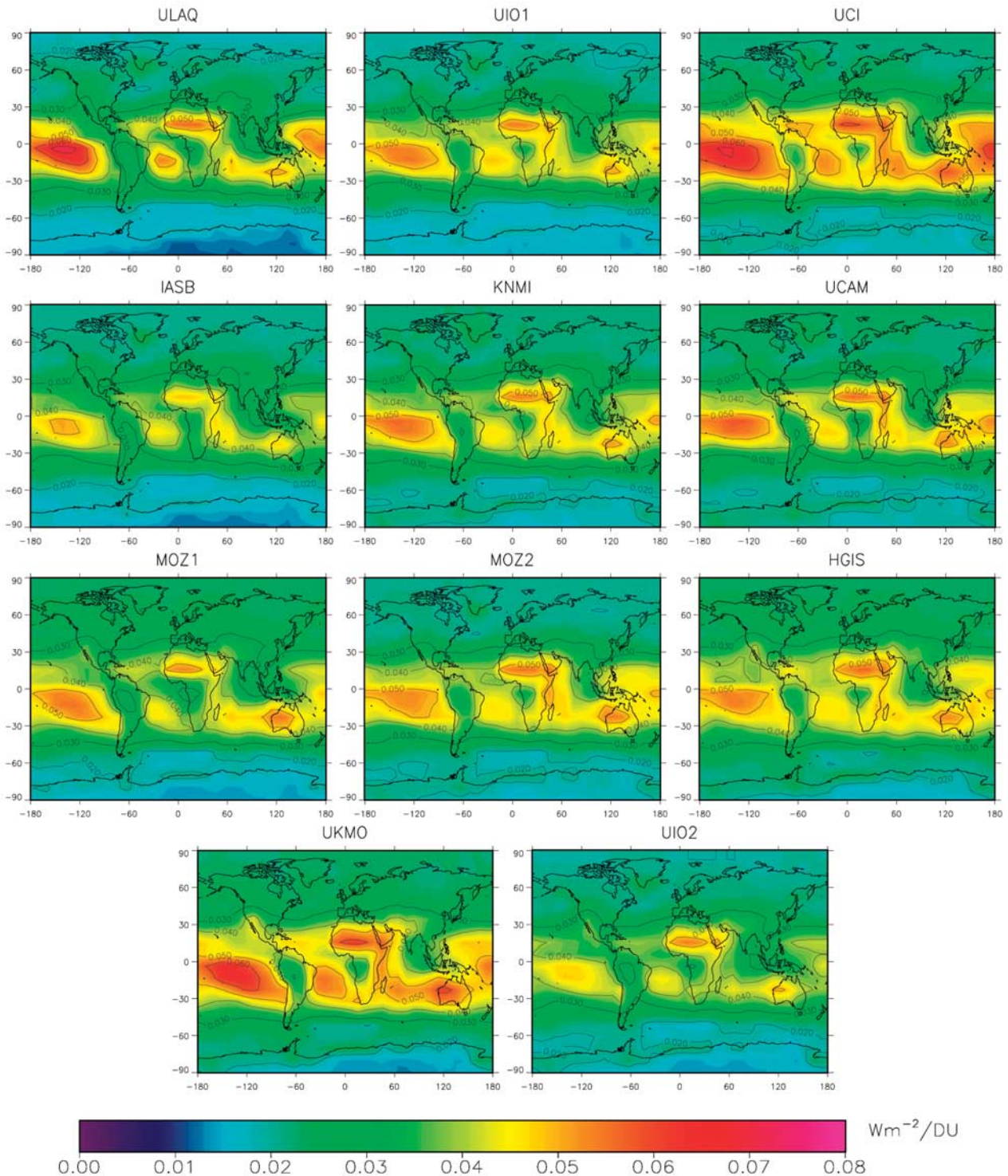


Figure 7. Same as Figure 6, but normalized, i.e., divided by the ozone column change ($\text{W m}^{-2} \text{DU}^{-1}$).

(see section 2.2.3) we obtain a radiative forcing of 0.77 W m^{-2} , reflecting the much smaller increases in lower stratospheric ozone, and a normalized radiative forcing of $0.031 \text{ W m}^{-2} \text{DU}$.

[57] For all the models the normalized radiative forcing decreases when ozone changes in the stratosphere are taken into account, except for MOZ2 where it remains nearly

unchanged (related to the very small stratospheric contribution in this model).

4. Concluding Remarks

[58] In this analysis ozone changes in the troposphere and lower stratosphere predicted by various CTMs for the

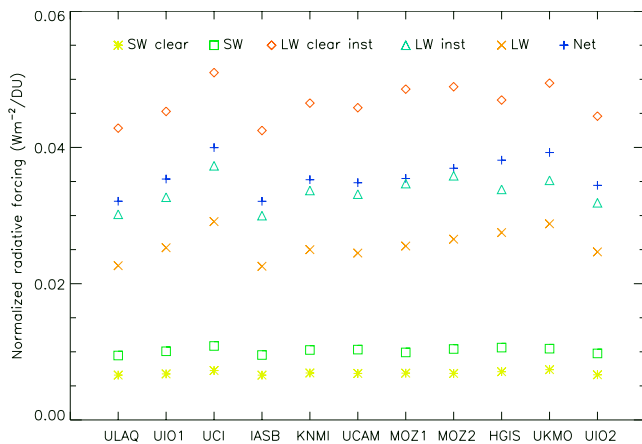


Figure 8. Normalized global mean radiative forcing due to changes in tropospheric ozone between 2000 and 2100 ($W m^{-2} DU^{-1}$), separated into shortwave (SW) and longwave (LW) components and calculated under different assumptions. Clear, clear-sky conditions; inst, no stratospheric temperature adjustment; and net, LW + SW.

period 2000–2100 based on the SRES A2p scenario are used to calculate radiative forcing. Calculations of the radiative forcing due to the increase in tropospheric ozone expected for the 21st century range from 0.40 to 0.78 $W m^{-2}$, the average being equal to 0.56 $W m^{-2}$. Compared with 5.6 $W m^{-2}$, the combined radiative forcing due to all well-mixed greenhouse gases in the SRES A2p scenario [Ramaswamy *et al.*, 2001], tropospheric ozone remains an important agent for radiative forcing in the future. As the SRES A2p scenario represents an upper estimate of ozone

Table 4. Radiative Transfer Calculations Based on Results From the Models Calculating Changes in the Stratosphere^a

Model	ΔO_3 , DU	SW RF, $W m^{-2}$	LW RF, $W m^{-2}$	RF, $W m^{-2}$	NRF, $W m^{-2} DU^{-1}$
ULAQ	27.8 (18.5)	0.10 (0.18)	0.67 (0.42)	0.78 (0.61)	0.028 (0.033)
UIO2	28.7 (21.2)	0.15 (0.22)	0.71 (0.50)	0.86 (0.71)	0.030 (0.033)
Mean	28.3 (19.9)	0.13 (0.20)	0.69 (0.46)	0.82 (0.66)	0.029 (0.033)

^aBoth tropospheric and stratospheric changes calculated by the models were taken into account. (Results with tropospheric changes only are given in parentheses. These are larger than the values in Table 3, because the larger increase in stratospheric ozone also implies larger ozone increase in the troposphere.) ΔO_3 , ozone column change; SW RF, shortwave radiative forcing; LW RF, longwave radiative forcing; RF, net radiative forcing; RF (NH/SH), ratio between radiative forcing in the Northern Hemisphere to radiative forcing in the Southern Hemisphere; NRF, normalized radiative forcing (all values are annually and globally averaged).

precursor emissions we consider the obtained radiative forcing to be an upper estimate as well.

[59] We apply the same radiative transfer model to all sets of modeled ozone changes, and the resulting normalized radiative forcing is within a relatively narrow range, between 0.032 and 0.040 $W m^{-2} DU^{-1}$, i.e., much narrower than the range reported in IPCC-TAR [Ramaswamy *et al.*, 2001]. The robustness of the normalized radiative forcing suggests that the global mean radiative forcing can be derived from the global mean ozone column change.

[60] The main uncertainty in the radiative forcing calculations arises from the differences in global mean ozone column change as simulated by the various CTMs. The contribution of the radiative forcing uncertainties caused by different ozone profile characteristics is of secondary importance, as reflected by the much smaller fluctuation among the normalized radiative forcing values. In particular, uncer-

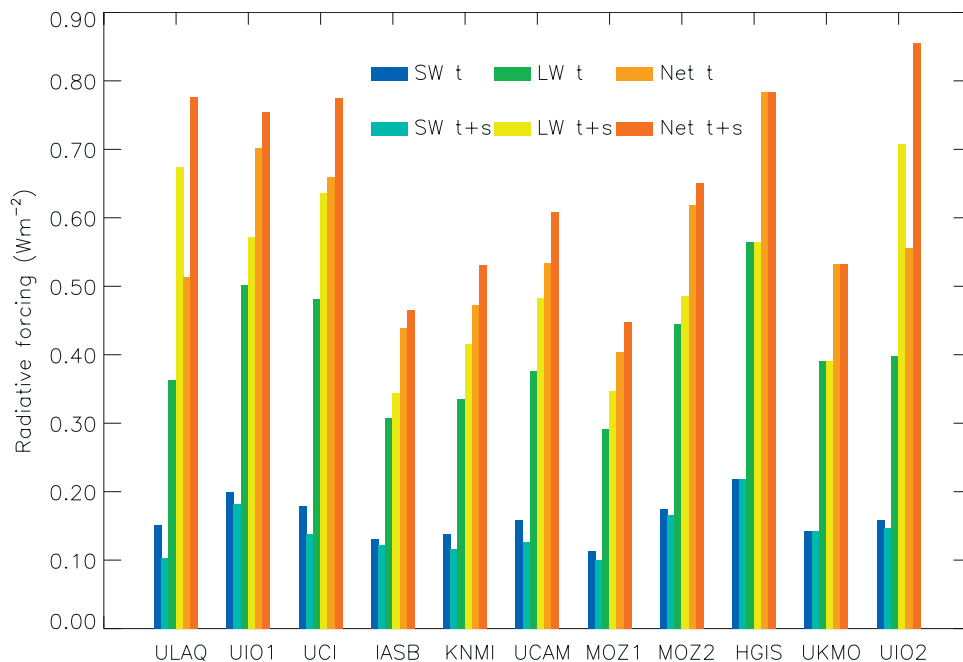


Figure 9. Components of global-mean radiative forcing for each model ($W m^{-2}$). SW, shortwave component; LW, longwave component; t, including tropospheric ozone changes only; and t + s, including both tropospheric and stratospheric changes. (Note: for ULAQ and UIO2 the t + s bars refer to the experiments calculating stratospheric ozone change discussed in section 2.2.)

tainties in the CTM calculations that were discussed in section 2 need to be resolved and emission scenarios have to be refined in order to get more accurate predictions for changes in ozone. Also, climate chemistry feedback mechanisms identified in various studies [e.g., Granier and Shine, 1999; Stevenson et al., 2000; Johnson et al., 1999, 2001; Grewe et al., 2001b] could not be included in the CTM simulations and this lack adds to the uncertainty in predicted ozone changes. Major identified feedback mechanisms include the change of chemical reaction rates due to tropospheric temperature increase and the enhanced photochemical destruction of tropospheric ozone related to the expected increases in water vapor. For example, Stevenson et al. [2000] find a radiative forcing due to tropospheric ozone increase between 1990 and 2100 amounting to 0.43 W m^{-2} , ignoring climate change. This value falls to 0.27 W m^{-2} when climate feedback on chemistry is included. These results indicate the potential importance of climate feedbacks on chemistry.

[61] The present study also addresses the radiative forcing due to ozone changes in the stratosphere. When changes in the lower stratosphere (up to 20 km altitude) are included, the radiative forcing due to ozone amounts to 0.82 W m^{-2} . The calculated normalized radiative forcing of $0.029 \text{ W m}^{-2} \text{ DU}^{-1}$ is somewhat lower than the value obtained in the tropospheric study and is related to the negative shortwave contribution from stratospheric ozone increase. Clearly, further model studies will be needed to investigate the contribution from the lower stratosphere to the radiative forcing. Also, more research is needed on feedbacks between stratospheric ozone chemistry and climate change, in particular, changes in stratospheric circulation, temperatures, and water vapor concentrations. As pointed out by several authors, climate change induced by greenhouse gases may have an impact on the timing of future ozone recovery [see for e.g., Shindell et al., 1998; Austin et al., 2000, 2002]. Based on the assumptions on future emissions and the model studies performed in IPCC-TAR and in this analysis, it can be concluded that the contribution of lower stratospheric ozone changes to the radiative forcing in the 21st century is likely to be a small but important fraction of the total.

[62] The relation between the spatially inhomogeneous radiative forcing due to ozone changes and the actual climate impact as evidenced, for instance, by changing surface temperatures, is not straightforward. The climate sensitivity (i.e., the expected surface temperature change per unit radiative forcing) can vary significantly depending on the ozone change profile and feedback mechanisms involving clouds and water vapor distribution [Hansen et al., 1997; Stuber et al., 2001]. This complexity does not negate the use of radiative forcing to derive climate change, but it adds further to the chain of uncertainty in predicting the role of ozone in 21st century climate change.

[63] **Acknowledgments.** The authors would like to thank the anonymous reviewers for numerous helpful comments.

References

- Austin, J., J. Knight, and N. Butchart, Three-dimensional chemical model simulations of the ozone layer: 1979–2015, *Q. J. R. Meteorol. Soc.*, **126**, 1533–1556, 2000.

- Austin, J., et al., Uncertainties and assessments of chemistry-climate models of the stratosphere, *Atmos. Chem. Phys. Discuss.*, **2**, 1035–1096, 2002.
- Bekki, S., K. S. Law, and J. A. Pyle, Effect of ozone depletion on atmospheric CH_4 and CO concentrations, *Nature*, **371**, 595–597, 1994.
- Berntsen, T. K., and I. S. A. Isaksen, A global 3-D chemical transport model for the troposphere, 1, Model description and CO and Ozone results, *J. Geophys. Res.*, **102**, 21,239–21,280, 1997.
- Berntsen, T. K., and I. S. A. Isaksen, Effects of lightning and convection on changes in tropospheric ozone due to NO_x emissions from aircraft, *Tellus, Ser. B*, **51**, 766–788, 1999.
- Berntsen, T. K., I. S. A. Isaksen, G. Myhre, J. S. Fuglestedt, F. Stordal, T. A. Larsen, R. S. Freckleton, and K. P. Shine, Effects of anthropogenic emissions on tropospheric ozone and its radiative forcing, *J. Geophys. Res.*, **102**, 28,101–28,126, 1997.
- Berntsen, T. K., G. Myhre, F. Stordal, and I. S. A. Isaksen, Time evolution of tropospheric ozone and its radiative forcing, *J. Geophys. Res.*, **105**, 8915–8930, 2000.
- Brasseur, G. P., J. T. Kiehl, J.-F. Müller, T. Schneider, C. Granier, X. X. Tie, and D. Hauglustaine, Past and future changes in global tropospheric ozone: Impact on radiative forcing, *Geophys. Res. Lett.*, **25**, 3807–3810, 1998a.
- Brasseur, G. P., D. A. Hauglustaine, S. Walters, P. J. Rasch, J.-F. Müller, C. Granier, and X. X. Tie, MOZART, a global chemical transport model for ozone and related chemical tracers, 1, Model description, *J. Geophys. Res.*, **103**, 28,265–28,289, 1998b.
- Brasseur, G. P., R. A. Cox, D. Hauglustaine, I. Isaksen, J. Leliveld, D. H. Lister, R. Sausen, U. Schumann, A. Wahner, and P. Wiesen, European scientific assessment of the atmospheric effects of aircraft emissions, *Atmos. Environ.*, **32**, 2329–2418, 1998c.
- Carslaw, K., B. Luo, and T. Peter, An analytic expression for the composition of aqueous $\text{HNO}_3 + \text{H}_2\text{SO}_4$ stratospheric aerosols including gas phase removal of HNO_3 , *Geophys. Res. Lett.*, **22**, 1877–1880, 1995.
- Chalita, S., D. A. Hauglustaine, H. Le Treut, and J.-F. Müller, Radiative forcing due to increased tropospheric ozone concentrations, *Atmos. Environ.*, **30**, 1641–1646, 1996.
- Collins, W. J., D. S. Stevenson, C. E. Johnson, and R. G. Derwent, Tropospheric ozone in a global-scale three-dimensional Lagrangian model and its response to NO_x emission controls, *J. Atmos. Chem.*, **26**, 223–274, 1997.
- Collins, W. J., D. S. Stevenson, C. E. Johnson, and R. G. Derwent, Role of convection in determining the budget of odd hydrogen in the upper troposphere, *J. Geophys. Res.*, **104**, 26,927–26,941, 1999.
- Costen, R. C., G. M. Tenille, and J. S. Levine, Cloud pumping in a one-dimensional photochemical model, *J. Geophys. Res.*, **93**, 15,941–15,954, 1988.
- Crutzen, P. J., M. G. Lawrence, and U. Poschl, On the background photochemistry of tropospheric ozone, *Tellus, Ser. AB*, **51**, 123–146, 1999.
- Del Genio, A. D., and M. S. Yao, Efficient cumulus parameterization for long-term climate studies: The GISS scheme, in *The Representation of Cumulus Convection in Numerical Models*, *AMS Monogr. Ser.*, edited by K. A. Emanuel and D. J. Raymond, Am. Meteorol. Soc., Boston, Mass., 1993.
- Del Genio, A. D., M.-S. Yao, W. Kovari, and K. K. W. Lo, A prognostic water parameterization for global climate models, *J. Clim.*, **9**, 270–304, 1996.
- De Winter-Sorkina, R., Impact of ozone layer depletion, I, Ozone depletion climatology, *Atmos. Environ.*, **35**, 1609–1614, 2001.
- Fishman, J., J. M. Hoell, R. D. Bendura, R. J. McNeil, and V. W. J. H. Kirchhoff, NASA GTE TRACE A experiment (September–October 1992): Overview, *J. Geophys. Res.*, **101**, 23,864–23,879, 1996.
- Forster, P. M. de F., Radiative forcing due to stratospheric ozone changes 1979–1997, using updated trend estimates, *J. Geophys. Res.*, **104**, 24,395–24,399, 1999.
- Forster, P. M. de F., and K. P. Shine, Radiative forcing and temperature trends from stratospheric ozone changes, *J. Geophys. Res.*, **102**, 10,841–10,857, 1997.
- Fuglestedt, J. S., J. E. Jonson, and I. S. A. Isaksen, Effects of reduction in stratospheric ozone on tropospheric chemistry through changes in photolysis rates, *Tellus, Ser. B*, **46**, 172–192, 1994.
- Fuglestedt, J. S., T. Berntsen, I. S. A. Isaksen, M. Liang, and W.-C. Wang, Climatic forcing of nitrogen oxides thorough changes in tropospheric ozone and methane; global 3-D model studies, *Atmos. Environ.*, **33**, 961–977, 1999.
- Giorgi, F., and W. L. Chameides, The rainout parameterization in a photochemical model, *J. Geophys. Res.*, **90**, 7872–7880, 1985.
- Graedel, T. E., et al., A compilation of inventories of emissions to the atmosphere, *Global Biogeochem. Cycles*, **7**, 1–26, 1993.
- Granier, C., and K. P. Shine, Climate effects of ozone and halocarbon changes, in *Scientific Assessment of Ozone Depletion: 1998, Rep. 44*, chap. 10, pp. 10.1–10.38, Global Ozone Res. and Monit. Proj., World Meteorol. Organ., Geneva, 1999.

- Grewe, V., D. Brunner, M. Dameris, J. L. Grenfell, R. Hein, D. Shindell, and J. Staehelin, Origin and variability of upper tropospheric nitrogen oxides and ozone at northern mid-latitudes, *Atmos. Environ.*, **35**, 3421–3433, 2001a.
- Grewe, V., M. Dameris, R. Hein, R. Sausen, and B. Steil, Future changes of the atmospheric composition and the impact of climate change, *Tellus, Ser. B*, **53**, 103–121, 2001b.
- Guelle, W., Y. J. Balkanski, J. E. Dibb, M. Schulz, and F. Dulac, Wet deposition in a global size-dependent aerosol transport model, 2, Influence of the scavenging scheme on Pb-210 vertical profiles, surface concentrations, and deposition, *J. Geophys. Res.*, **103**, 28,875–28,891, 1998.
- Hack, J. J., Parameterization of moist convection in the NCAR community climate model (CCM2), *J. Geophys. Res.*, **99**, 5551–5568, 1994.
- Hansen, J., M. Sato, and R. Ruedy, Radiative forcing and climate response, *J. Geophys. Res.*, **102**, 6831–6864, 1997.
- Hauglustaine, D. A., and G. P. Brasseur, Evolution of tropospheric ozone under anthropogenic activities and associated radiative forcing of climate, *J. Geophys. Res.*, **106**, 32,337–32,360, 2001.
- Hauglustaine, D. A., G. P. Brasseur, S. Walters, P. J. Rasch, J.-F. Müller, L. K. Emmons, and M. A. Carroll, MOZART, a global chemical transport model for ozone and related chemical tracers, 2, Model results and evaluation, *J. Geophys. Res.*, **103**, 28,291–28,335, 1998.
- Haywood, J. M., M. D. Schwarzkopf, and V. Ramaswamy, Estimates of radiative forcing due to modeled increases in tropospheric ozone, *J. Geophys. Res.*, **103**, 16,999–17,007, 1998.
- Hofmann, D. J., and J. A. Pyle, Predicting future ozone changes and detection of recovery, in *Scientific Assessment of Ozone Depletion: 1998*, Rep. 44, chap. 12, pp. 12.1–57, Global Ozone Res. and Monit. Proj., World Meteorol. Org., Geneva, 1999.
- Houweling, S., F. Dentener, J. Lelieveld, B. Walter, and E. Dlugokencky, The modeling of tropospheric methane: How well can point measurements be reproduced by a global model?, *J. Geophys. Res.*, **105**, 8981–9002, 2000.
- Isaksen, I. S. A., and Ø. Hov, Calculations of trends in the tropospheric concentrations of O₃, OH, CO, CH₄, and NO_x, *Tellus, Ser. B*, **39**, 271–283, 1987.
- Isaksen, I. S. A., and C. Jackman, Modeling the chemical composition of the future atmosphere, in *Aviation and the Global Atmosphere*, edited by J. E. Penner et al., chap. 4, pp. 121–183, Cambridge Univ. Press, New York, 1999.
- Jacob, D. J., et al., Evaluation and intercomparison of global atmospheric transport models using ²²²Rn and other short-lived tracers, *J. Geophys. Res.*, **102**, 5953–5970, 1997.
- Jeuken, A. B. M., H. J. Eskes, P. F. J. van Velthoven, H. M. Kelder, and E. V. Hölm, Assimilation of total ozone satellite measurements in a three-dimensional tracer transport model, *J. Geophys. Res.*, **104**, 5551–5563, 1999.
- Johnson, C. E., W. J. Collins, D. S. Stevenson, and R. G. Derwent, The relative roles of climate and emissions changes on future oxidant concentrations, *J. Geophys. Res.*, **104**, 18,631–18,645, 1999.
- Johnson, C. E., D. S. Stevenson, W. J. Collins, and R. G. Derwent, Role of climate feedback on methane and ozone studied with a coupled Ocean-Atmosphere-Chemistry model, *Geophys. Res. Lett.*, **28**, 1723–1726, 2001.
- Karlsdottir, S., I. S. A. Isaksen, G. Myhre, and T. K. Berntsen, Trend analysis of O₃ and CO in the period 1980 to 1996: A 3-D model study, *J. Geophys. Res.*, **105**, 28,907–28,933, 2000.
- Kiehl, J. T., T. L. Schneider, R. W. Portmann, and S. Solomon, Climate forcing due to tropospheric and stratospheric ozone, *J. Geophys. Res.*, **104**, 31,239–31,254, 1999.
- Kinne, S., et al., Monthly averages of aerosol properties: A global comparison among models, satellite data, and AERONET ground data, *J. Geophys. Res.*, **108**, doi:10.1029/2001JD001253, in press, 2003.
- Koch, D., D. Jacob, I. Tegen, D. Rind, and M. Chin, Tropospheric sulfur simulation and sulfate direct radiative forcing in the GISS GCM, *J. Geophys. Res.*, **104**, 23,799–23,822, 1999.
- Lacis, A. A., D. J. Wuebbles, and J. A. Logan, Radiative forcing by changes in the vertical distribution of ozone, *J. Geophys. Res.*, **95**, 9971–9981, 1990.
- Law, K. S., P.-H. Plantévin, D. E. Shallcross, H. L. Rogers, J. A. Pyle, C. Grouhel, V. Thouret, and A. Marengo, Evaluation of modeled O₃ using MOZIC data, *J. Geophys. Res.*, **103**, 25,721–25,740, 1998.
- Law, K. S., P.-H. Plantévin, V. Thouret, A. Marengo, W. A. H. Asman, M. Lawrence, P. J. Crutzen, J. F. Müller, D. A. Hauglustaine, and M. Kanakidou, Comparison between global chemistry transport model results and MOZIC data, *J. Geophys. Res.*, **105**, 1503–1525, 2000.
- Lelieveld, J., and P. J. Crutzen, Role of deep convection in the ozone budget of the troposphere, *Science*, **264**, 1759–1761, 1994.
- Lin, S.-J., and R. B. Rood, Multidimensional flux-form semi-Lagrangian transport schemes, *Mon. Weather Rev.*, **124**, 2046–2070, 1996.
- McPeters, R. D., S. M. Hollandsworth, L. E. Flynn, J. R. Herman, and C. J. Seftor, Long-term ozone trends derived from the 16-year combined Nimbus 7/Meteor 3 TOMS version 7 record, *Geophys. Res. Lett.*, **23**, 3699–3702, 1996.
- Mickley, L. J., P. P. Murti, D. J. Jacob, J. A. Logan, D. Rind, and D. Koch, Radiative forcing from tropospheric ozone calculated with a unified chemistry-climate model, *J. Geophys. Res.*, **104**, 30,153–30,172, 1999.
- Mickley, L. J., D. J. Jacob, and D. Rind, Uncertainty in preindustrial abundance of tropospheric ozone: Implications for radiative forcing calculations, *J. Geophys. Res.*, **106**, 3389–3399, 2001.
- Müller, J.-F., and G. Brasseur, IMAGES: A three-dimensional chemical transport model of the global troposphere, *J. Geophys. Res.*, **100**, 16,445–16,490, 1995.
- Müller, J.-F., and G. Brasseur, Sources of upper tropospheric HO₂: A three-dimensional study, *J. Geophys. Res.*, **104**, 1705–1715, 1999.
- Myhre, G., S. Karlsdóttir, I. S. A. Isaksen, and F. Stordal, Radiative forcing due to changes in tropospheric ozone in the period 1980 to 1996, *J. Geophys. Res.*, **105**, 28,935–28,942, 2000.
- Myhre, G., A. Myhre, and F. Stordal, Historical evolution of radiative forcing of climate, *Atmos. Environ.*, **35**, 2361–2373, 2001.
- Nakicenovic, N., et al., *Emissions Scenarios, A Special Report of Working Group III of the Intergovernmental Panel on Climate Change*, 599 pp., Cambridge Univ. Press, New York, 2000.
- Olivier, J. G. J., A. F. Bouwman, K. W. Van der Hoek, and J. J. M. Berdowski, Global air emission inventories for anthropogenic sources of NO_x, NH₃ and N₂O in 1990, *Environ. Pollut.*, **102**, 135–148, 1998.
- Olivier, J. G. J., A. F. Bouwman, J. J. M. Berdowski, C. Veldt, J. P. J. Bloos, A. J. H. Visschedijk, C. W. M. Van der Maas, and P. Y. J. Zandveld, Sectoral emission inventories of greenhouse gases for 1990 on a per country basis as well as on 1 × 1, *Environ. Sci. Policy*, **2**, 241–263, 1999.
- Penner, J. E., C. S. Atherton, J. Dignon, S. J. Ghan, J. J. Walton, and S. Hameed, Global emissions and models of photochemically active compounds, in *Global Atmospheric Biospheric Chemistry*, edited by R. G. Prinn, pp. 223–247, Plenum, New York, 1994.
- Pitari, G., A numerical study of the possible perturbation of stratospheric dynamics due to Pinatubo aerosols—Implications for tracer transport, *J. Atmos. Sci.*, **50**, 2443–2461, 1993.
- Pitari, G., E. Mancini, V. Rizi, and D. T. Shindell, Impact of future climate and emission changes on stratospheric aerosols and ozone, *J. Atmos. Sci.*, **59**, 414–440, 2002.
- Prather, M. J., Numerical advection by conservation of second-order moments, *J. Geophys. Res.*, **91**, 6671–6681, 1986.
- Prather, M. J., and D. J. Jacob, A persistent imbalance in HO_x and NO_x photochemistry of the upper troposphere driven by deep tropical convection, *Geophys. Res. Lett.*, **24**, 3189–3192, 1997.
- Prather, M. J., M. McElroy, S. Wofsy, G. Russel, and D. Rind, Chemistry of the global troposphere: Fluorocarbons as tracers of air motion, *J. Geophys. Res.*, **92**, 6579–6613, 1987.
- Prather, M. J., et al., Atmospheric chemistry and greenhouse gases, in *Climate Change 2001: The Scientific Basis. Contribution of Working Group I to the Third Assessment Report of the Intergovernmental Panel on Climate Change (IPCC)*, edited by J. T. Houghton et al., 881 pp., Cambridge Univ. Press, New York, 2001.
- Prinn, R. G., et al., Evidence of substantial variations of atmospheric hydroxyl radicals in the past two decades, *Science*, **292**, 1882–1888, 2001.
- Ramaswamy, V., O. Boucher, J. Haigh, D. Hauglustaine, J. Haywood, G. Myhre, T. Nakajima, G. Y. Shi, and S. Solomon, Radiative forcing of climate change, in *Climate Change 2001: The Scientific Basis. Contribution of Working Group I to the Third Assessment Report of the Intergovernmental Panel on Climate Change (IPCC)*, edited by J. T. Houghton et al., 881 pp., Cambridge Univ. Press, New York, 2001.
- Roelofs, G. J., Radiative forcing by tropospheric ozone: Impact of cloud representation, *Geophys. Res. Lett.*, **26**, 467–470, 1999.
- Rummukainen, M., I. S. A. Isaksen, B. Rognerud, and F. Stordal, A global model tool for three-dimensional multiyear stratospheric chemistry simulations: Model description and first results, *J. Geophys. Res.*, **104**, 26,437–26,456, 1999.
- Russel, G. L., and J. A. Lerner, A finite difference scheme for the tracer transport equation, *J. Appl. Meteorol.*, **20**, 1483, 1981.
- Shindell, D. T., D. Rind, and P. Lonergan, Increased polar stratospheric ozone losses and delayed eventual recovery owing to increasing greenhouse-gas concentrations, *Nature*, **392**(6676), 589–592, 1998.
- Smolarkiewicz, P. K., and P. J. Rasch, Monotone advection on the sphere: An Eulerian versus semi-Lagrangian approach, *J. Atmos. Sci.*, **48**, 793–810, 1991.
- Stevenson, D. S., C. E. Johnson, W. J. Collins, R. G. Derwent, K. P. Shine, and J. M. Edwards, Evolution of tropospheric ozone radiative forcing, *Geophys. Res. Lett.*, **25**, 3819–3822, 1998a.
- Stevenson, D. S., W. J. Collins, C. D. Johnson, and R. G. Derwent, Intercomparison and evaluation of atmospheric transport in a Lagrangian

- model (STOCHEM) and an Eulerian model (UM), using 222-Rn as a short-lived tracer, *Q. J. R. Meteorol. Soc.*, 125, 2477–2493, 1998b.
- Stevenson, D. S., C. E. Johnson, W. J. Collins, R. G. Derwent, and J. M. Edwards, Future tropospheric ozone radiative forcing and methane turnover—The impact of climate change, *Geophys. Res. Lett.*, 27, 2073–2076, 2000.
- Stockwell, D. Z., and M. P. Chipperfield, A tropospheric chemical-transport model: Development and validation of the model transport schemes, *Q. J. R. Meteorol. Soc.*, 125(557), 1747–1783, 1999.
- Stuber, N., M. Ponater, and R. Sausen, Is the climate sensitivity to ozone perturbations enhanced by stratospheric water vapor feedback?, *Geophys. Res. Lett.*, 28, 2887–2890, 2001.
- Sundet, J. K., Model studies with a 3-D global CTM using ECMWF data, Ph.D. thesis, Dep. of Geophys., Univ. of Oslo, Oslo, Norway, 1997.
- Tiedtke, M., A comprehensive mass flux scheme for cumulus parameterisation on large scale models, *Mon. Weather Rev.*, 117, 1779–1800, 1989.
- van Dorland, R., F. J. Dentener, and J. Lelieveld, Radiative forcing due to tropospheric ozone and sulfate aerosols, *J. Geophys. Res.*, 102, 28,079–28,100, 1997.
- Wang, W.-C., and N. D. Sze, Coupled effects of atmospheric N₂O and O₃ on the Earth's atmosphere, *Nature*, 286, 589–590, 1980.
- Wang, Y., D. J. Jacob, and J. A. Logan, Global simulation of tropospheric O₃-NO_x-hydrocarbon chemistry, 1, Model formulation, *J. Geophys. Res.*, 103, 10,713–10,725, 1998.
- Wennberg, P. O., et al., Removal of stratospheric O₃ by radicals: In situ measurements of OH, HO₂, NO, NO₂, ClO, and BrO, *Science*, 266, 398–404, 1994.
- Wild, O., and H. Akimoto, Intercontinental transport of ozone and its precursors in a three-dimensional global CTM, *J. Geophys. Res.*, 106, 27,729–27,744, 2001.
- Wild, O., and M. J. Prather, Excitation of the primary tropospheric chemical mode in a global CTM, *J. Geophys. Res.*, 105, 24,647–24,660, 2000.
- Williamson, D. L., and P. J. Rasch, Two-dimensional semi-Lagrangian transport with shape preserving interpolation, *Mon. Weather Rev.*, 117, 102–129, 1989.
- World Meteorological Organization (WMO), Scientific assessment of ozone depletion: 1998, *Rep. 44*, 732 pp., Global Ozone Res. and Monit. Proj., Geneva, 1999.
- Zhang, G. J., and N. A. McFarlane, Sensitivity of climate simulations to the parameterization of cumulus convection in the Canadian Climate Centre general circulation model, *Atmos. Ocean*, 33, 407–446, 1995.

T. K. Berntsen, M. Gauss, I. S. A. Isaksen, G. Myhre, and J. K. Sundet, Department of Geophysics, University of Oslo, P.O. 1022, Blindern, 0315 Oslo, Norway. (michaelg@geofysikk.uio.no)

G. P. Brasseur, Max-Planck-Institut für Meteorologie, 20146 Hamburg, Germany.

F. J. Dentener, Joint Research Centre, Climate Change Unit, 21020 Ispra, Italy.

R. G. Derwent, UK Met Office, Climate Research Division, Berks RG12 2SZ, UK.

D. A. Hauglustaine, Institut Pierre Simon Laplace (IPSL), 91191 Gif-sur-Yvette, France.

L. W. Horowitz, GFDL, NOAA, Princeton University, Princeton, NJ 08540, USA.

D. J. Jacob and L. J. Mickley, Department of Earth and Planetary Sciences, Harvard University, Cambridge, MA 02138, USA.

M. Johnson, K. S. Law, P.-H. Plantévin, J. A. Pyle, and H. L. Rogers, Cambridge University, Chemistry Department, Cambridge CB2 1TN, UK. J.-F. Müller, IASB, 1180 Brussels, Belgium.

G. Pitari, Dipartimento di Fisica, Università de L'Aquila, 67010 Coppito, L'Aquila, Italy.

M. J. Prather, Earth System Science Department, University of California at Irvine, Irvine, CA 92697, USA.

D. S. Stevenson, Institute for Meteorology, University of Edinburgh, Edinburgh EH8 9YL, UK.

M. van Weele, Royal Netherlands Meteorological Institute (KNMI), 3730 De Bilt, Netherlands.

O. Wild, Frontier Research System for Global Change (FRSGC), Yokohama, 236-0001 Kanazawaku, Japan.